A Transient Two-dimensional CFD Evaluation of Indoor Thermal Comfort with an Intermittently-operated Radiant Floor Heating System in an Office Building

Jiying Liu[1,2,*], Xuwei Zhu[1], Moon Keun Kim[3], Ping Cui[1], Shengwei Zhu[4] and Risto Kosonen[5]

[1]School of Thermal Engineering, Shandong Jianzhu University, Jinan 250101, China; [2]Shandong Ground Source Heat Pump Engineering Research Center, Shandong GRAD Group, Dezhou 253000, China; [3]Department of Architecture, Xi'an Jiaotong – Liverpool University, Suzhou 215123, China; [4]Department of Mechanical Engineering, University of Maryland, College Park, MD 20740, USA and [5]Department of Mechanical Engineering, Aalto University, Espoo 00076, Finland

Abstract: To provide excellent thermal comfort in an energy-efficient manner, the radiant floor cooling and heating system has become an attractive technology. In this work, an intermittently-operated radiant floor heating system combined with a ventilation system for use during the weekdays is proposed via a transient two-dimensional computational fluid dynamics model that takes into account the variation of the indoor heat gain. Additionally, intermittent controls based on the minimum outdoor air temperature and the average water supply and return temperature are proposed. Six specifically-designed outdoor air temperature values ranging from -15°C to 15°C are taken as examples to evaluate the thermal comfort performance using the operative temperature and local thermal discomfort criteria, including the vertical air temperature, floor temperature, and radiant asymmetry. Meanwhile, the percentages dissatisfied induced by the local discomfort parameters above were analyzed.. Results show that for the case with a minimum outdoor air temperature of -14.2 °C, the earlier shut-off of the water supply (e.g., 18:00) cannot contribute to maintaining a comfortable environment at 7:00. To eliminate the effect of the indoor heat gain, a water supply shut-off after 20:00 and the pump starting to recirculate water in the concrete slab at 00:00 are encouraged in the case of an insufficient indoor heat gain during the next daytime. The maximum operative temperature commonly occurred between 4:00-6:00 p.m. A trade-off between the percentages dissatisfied and the operative temperature is finally identified. The control strategy of the shut-off of the water supply for two hours at noon and at least four hours during the nighttime is ultimately obtained to yield the acceptable thermal comfort performance in the intermittent operating mode of a floor heating system while effectively reducing energy consumption.

Keywords: Radiant floor heating system, Intermittent heating, Thermal comfort, Convective heat gain, Computational fluid dynamics.

1. INTRODUCTION

With the acceleration of urbanization, building energy consumption has been paid more and more attention [1, 2]. The rapid urbanization of the world caused changes to global energy use patterns and building-related carbon emissions [3, 4]. Therefore, the low-carbon energy development mode, utilization of renewable energy, and more efficient heating, ventilation and air conditioning (HVAC) system are effective ways to solve the problem of energy shortages [5, 6]. Radiant floor cooling and heating systems have been extensively studied due to their high level of thermal comfort and energy-saving potential as compared to conventional systems [7-10]. Due to the high thermal mass of building structures and possible intermittent use [11, 12], especially for office buildings, an optimal control strategy for floor heating systems integrated with the thermal mass of building should better be taken into account to enhance thermal comfort and reduce energy use [13, 14].

The operation mode of an intermittently-operated control strategy for radiant floor heating systems can be designed to effectively utilize the thermal storage of concrete floors [15-17]. Cho and Zaheer-Uddin [18] proposed a forecast of the outdoor air temperature and implemented an intermittent predictive control strategy in a residential building using TRNSYS software, and achieved an energy reduction of between 10% and 12% during the cold winter season. Yeom *et al*. [19] provided a control strategy for residential energy demand and achieved an approximate 4% reduction in heating energy consumption as compared to the conventional fixed-temperature and outdoor temperature reset control method. Shin *et al*. [20] proposed an occupancy inference method that was used for the optimal start and stop control of radiant floor heating systems. The results showed that the optimal start and stop control can reduce the heating energy consumption by up to 3.1% and thermal discomfort times from 62.5 h to 8.3 h. Gwerder *et al*. [21] utilized an intermittent operation with pulse width modulation accounting for the automatic switching between cooling and heating modes for variable comfort criteria, and conducted a laboratory test to outline the operation procedure.

*Address correspondence to this author at the School of Thermal Engineering, Shandong Jianzhu University, #1000 Fengming Road, Jinan 250101, China; E-mail: jxl83@sdjzu.edu.cn

E-ISSN: 2409-9821/20

Most previous studies accounted for the outdoor climatic conditions and the intermittent characteristic of the building type, especially residential buildings [22]; however, evaluations of fluctuating thermal comfort due to varying outdoor and indoor climatic conditions were not carefully considered [23]. Moreover, an air ventilation system should be used in conjunction with a radiant floor heating system in an office building, which significantly affects the indoor thermal environment, e.g., vertical temperature stratification and thermal comfort. The vertical air temperature difference is attributed to the effect of the radiant heating system that can be combined with a displacement ventilation system with lower-temperature supply air, thereby effectively extending the free cooling period of the air ventilation system [24]. From this perspective, the numerical method could be an alternative way to evaluate both thermal comfort and indoor thermal stratification while taking into account the transient internal usage and outdoor climatic conditions [25-27].

Numerical modeling has previously been used to assess thermal comfort or provide accurate boundary information for the energy consumption of radiant heating systems in full-scale building models [28, 29]. Gao *et al*. [30] used the three-dimensional (3D) modeling to investigate the differences of vertical air temperature gradients and thermal homogeneity across the floor for different layouts of under-floor heating pipes. Zheng *et al*. [31] established the 3D heat transfer model of a radiant floor heating system using the computational fluid dynamics (CFD) method to calculate the floor surface temperature, and analyze the effect of non-heating surface temperature on the heat output. Despite the realism and accuracy of 3D modeling for radiant floor systems, increasing the details of the physics of a model will inevitably increase the computational effort [32]. Moreover, this radiant floor system implies the use of thermal mass resulting in transient simulation required to represent the accuracy of system performance.

Therefore, the two-dimensional (2D) numerical modeling is an important tool to prevent a high computational effort, considering the symmetry of boundary conditions and specific assumptions of uniform and isotropic for building materials and heat transfer. Tye-Gingras and Gosselin [33] employed a 2D model coupled with a semi-analytic radiant panel model to optimize a radiant ceiling and wall hydronic radiant panel system in a typical residential building. Karabay *et al*. [34] conducted a 2D numerical investigation of fluid flow and heat transfer inside a room for floor-heating and wall-heating systems to compare their system performance. Zhang *et al*. [35] constructed a 2D model to analyze the performance of a radiant floor heating system under a transient external climatic condition and obtained a pre-heating control strategy during a weekend. Romani *et al*. [32] developed a transient 2D numeric model for radiant walls by validating with experimental data of a house-like cubicle and proposed intermittent heating control strategies with different supply periods from 0.5 h to 12 h. However, this study neglected the indoor geometry model and assumed a constant indoor air temperature of 21 ^{o}C.

Through literature review, this study reveals that several studies of 2D numerical modeling have been carried out due to the significant computational resources required for the 3D modeling, especially under transient conditions. However, few studies have considered the practical application of a radiant floor heating system combined with an outdoor air system operated intermittently and operates within certain thermal comfort limits. Moreover, the effect of internal heat gains in an office building has not been sufficiently accounted for in existing numerical models.

Therefore, the novelty of this study is to provide an intermittent operation strategy during the weekday. A 2D building model is created based on an existing office building. The indoor climatic conditions, including the ventilation condition and internal convective heat gains, are taken into account. The effect of solar radiation on the building enclosure is also considered. The thermal comfort is comprehensively evaluated using the operative temperature (T_{op}) and local thermal comfort criteria [36], including the vertical air temperature ($\Delta T_{0.1–1.1}$), floor temperature (T_{fl}), and radiant asymmetry (ΔT_{pr}). Moreover, the percentages dissatisfied (PDs) due to the discomfort parameters are compared. A proposed intermittent control strategy is ultimately obtained based on the relationship between the average water supply and return temperature (T_{ave}) and the minimum outdoor air temperature ($T_{min,out}$) in a cold climate zone to effectively reduce energy consumption.

2. METHODOLOGY

In this section, a 2D building enclosure model is presented that is used to evaluate the performance of the radiant floor heating system. The numerical method is introduced with boundary and internal climatic conditions. The proposed intermittent control strategy and meteorological data are also presented. Moreover, the indices of the thermal comfort evaluation are presented. CFD validations are finally conducted via

comparisons with the mixed convection determined by an experiment and the transient flow in a heat-releasing process determined by a field study.

2.1. Model Description and Geometry Assumption

In this study, a 2D building enclosure model of a radiant floor heating system combined with a ventilation system was proposed as shown in Figure **1**. This is a schematic representation of a typical office room with indoor heat gains and exterior/interior envelopes taking into account solar radiation, conduction, and convection heat transfer.

The selection of an office building model presented in Figure **2** was based on previous studies [17, 35, 37]. A simplified 2D model was constructed, and exterior window areas were assumed to be uniformly distributed along the exterior wall in the crosswise section. Moreover, the effect of interior walls in the spanwise direction on the indoor environment was neglected. In the modeling of the radiant floor, it was assumed symmetry conditions, constant fluid temperature, and homogenous thermal thermophysical properties along the water flow direction.

The 2D building model is illustrated in Figure **3**. The original office building model had a 3D size of 6.4×4.3×4.0 m (L×W×H) with a 2D interior room size of 5.8×3.5 m (L×H). The corresponding building envelope thicknesses for the exterior wall, exterior roof, interior

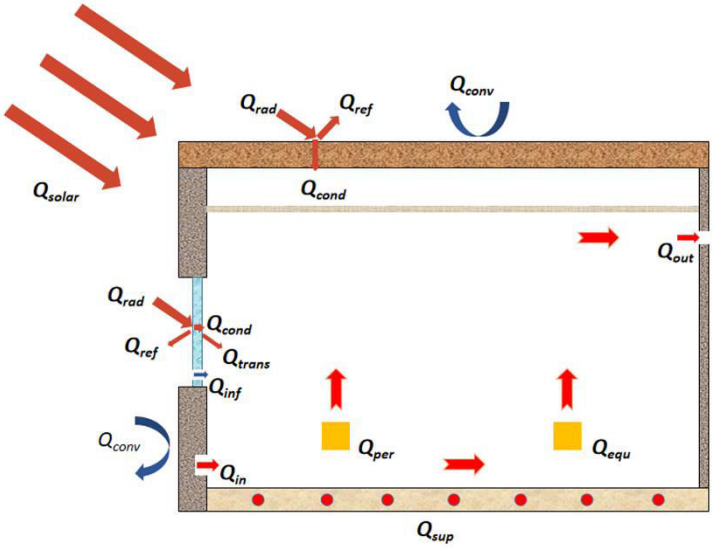

Figure 1: Schematic representation of a building model of a typical office room with a heating system (Q_{rad}: solar radiation, Q_{ref}: reflected solar radiation, Q_{conv}: convective heat transfer, Q_{cond}: conducted heat, Q_{inf}: infiltrated heat, Q_{per}: heat gain of occupant, Q_{equ}: heat gain of equipment, Q_{in}: air supply heat, Q_{sup}: water supply heat).

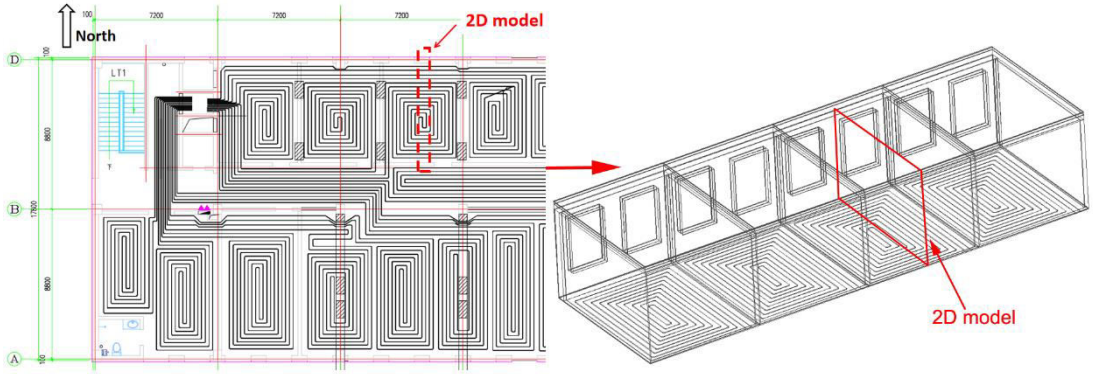

Figure 2: Simplification of a 2D geometric model of a case study office building [35].

wall, and interior floor were 365 mm, 340 mm, 240 mm, and 270 mm, respectively. To meet the Chinese design standard for the energy efficiency of public buildings [38], the U-values of 0.50 W/(m^2·K) and 0.45 W/(m^2·K) for the exterior wall and roof were respectively used. A double-glazed window with a 12-mm-thick air layer with a U-value of 2.4 W/(m^2·K) was utilized. The thermophysical parameters of the building components are given in Table **1**.

Figure **4** presents the schematic representation of the geometry of the heated floor structure. Three layers from outside to inside were structured above the ceiling adjacent and included a 20-mm-thick insulation layer, a 40-mm-thick light concrete layer, and a 20-mm-thick

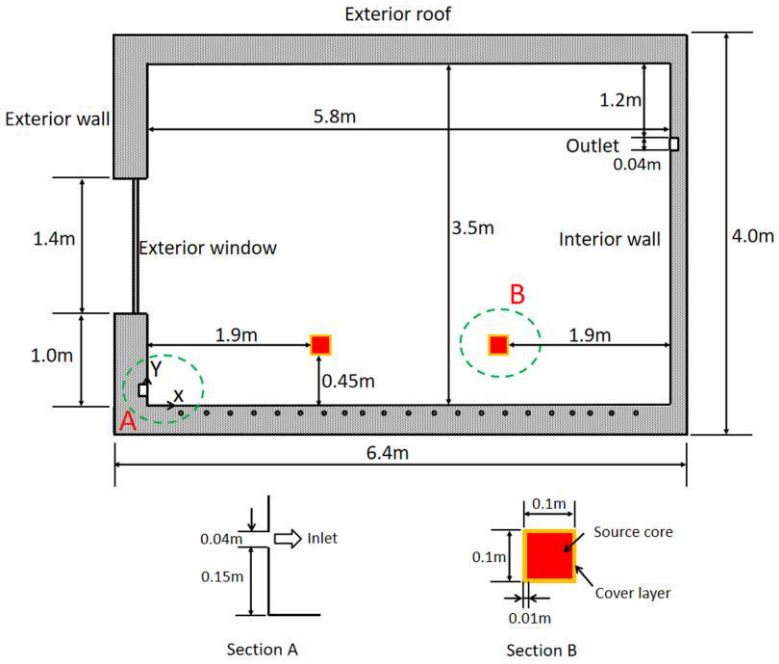

Figure 3: CFD geometry model of a 2D simulation case with separate sections describing the supply diffuser (section A) and indoor heat gain (section B).

Table 1: Thermophysical Parameters of the Building Components

Building Enclosure	Components (Inside to Outside)	Thickness (mm)	Density (kg/m^3)	Conductivity (W/m·K)	Specific Heat (J/kg·K)
Exterior wall	Mortar Concrete Mortar Insulation	20 300 20 25	1780 800 1800 30	0.94 0.41 0.94 0.024	1060 1350 1060 2400
Exterior roof	Concrete Mortar Insulation Mortar Brick	200 20 80 20 20	2400 1780 25 1780 1350	1.81 0.94 0.043 0.94 0.72	950 1060 5250 1060 1100
Exterior window*	Glazing Air Glazing	5 12 5	2400 1.24 2400	1.5 0.045 1.5	850 1006 850
Interior wall	Mortar Brick Mortar	20 200 20	1780 1350 1780	0.94 0.72 0.94	1060 1100 1060
Floor	Tile Light concrete Pipe embedded Insulation Concrete	20 40 2 20 200	2000 1200 1050 35 2400	2.1 1.45 0.4 0.022 1.81	950 1000 1000 4600 950

*A double-glazed window with an air layer was used, and the equivalent heat transfer coefficient of 2.4 W/(m^2·K) was designed for numerical simulation.

cover layer. An inner pipe diameter of 16 mm and a pipe spacing of 220 mm were used. A 2-mm-thick pipe with a thermal conductivity of 0.4 W/(m·K) was considered. A thermally-insulated office building model with a radiant floor-cooling/heating system and a constant-air-volume ventilation system was finally designed.

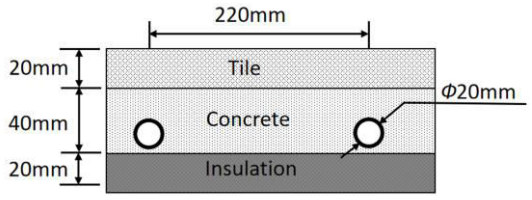

Figure 4: The schematic representation of the geometry of the floor structure.

2.2. Numerical Simulation

2.2.1. Model Description

Transient numerical simulations were carried out by ANSYS Fluent 16.1 software based on the finite volume method [39]. The shear-stress transport (SST) *k-ω* turbulence model was used to solve the continuity, momentum, and energy equations [40], which enhanced the performance of standard *k-ω* in modeling the near region of wall surfaces, and combined the advantages of the k-ε model in simulating the flow field in the outer region [41]. The transport equation of turbulence kinetic energy *k* and specific turbulence dissipation rate *ω* are calculated through Eq. (1) and (2).

$$\frac{\partial(\rho \mathrm{k})}{\partial \mathrm{t}}+\frac{\partial\left(\rho \mathrm{U}_{\mathrm{j}} \mathrm{k}\right)}{\partial \mathrm{x}_{\mathrm{j}}}=\frac{\partial}{\partial \mathrm{x}_{\mathrm{j}}}\left(\left(\mu+\frac{\mu_{\mathrm{t}}}{\sigma_{\mathrm{k}}}\right) \frac{\partial \mathrm{k}}{\partial \mathrm{x}_{\mathrm{j}}}\right)+\widetilde{\mathrm{G}_{\mathrm{k}}}-\mathrm{Y}_{\mathrm{k}}+\mathrm{S}_{\mathrm{k}} \quad (1)$$

$$\frac{\partial(\rho \omega)}{\partial t}+\frac{\partial\left(\rho U_j \omega\right)}{\partial x_j}=\frac{\partial}{\partial x_j}\left(\left(\mu+\frac{\mu_t}{\sigma_k}\right) \frac{\partial \omega}{\partial x_j}\right)+G_\omega-Y_\omega+D_\omega+S_\omega \quad (2)$$

where $\widetilde{G_k}$ is the production of *k* due to mean velocity gradients, G_ω is the generation of *ω*, Y_k and Y_ω are the dissipations of *k* and *ω* due to the turbulence, respectively, D_ω is the cross-diffusion term, S_k and S_ω are the under-defined source terms for *k* and *ω*, respectively, σ_k and σ_ω are the turbulent Prandtl numbers for *k* and *ω*, respectively. The turbulence viscosity (μ_t) is correlated to *k* and *ω* given by Eqs. (3)-(6).

$$\mu_t=\rho \frac{k}{\omega} \frac{1}{max\left[\frac{1}{\alpha^* a_1 \omega}\right]} \quad (3)$$

$$\alpha^*=\alpha_\infty^*\left(\frac{\alpha_0^*-1}{1+\frac{\rho k}{6 \mu \omega}}+1\right) \quad (4)$$

$$F_2=\tanh\left(\emptyset^2\right) \quad (5)$$

$$\emptyset=max\left(\frac{2k^{0.5}}{0.09\omega y}, \frac{500\mu}{\rho y^2 \omega}\right) \quad (6)$$

where *S* is the strain rate magnitude, F_2 is the blending function, *y* is the distance to the nearest wall surface. The model constants of a_1, α_∞^*, and α_0^* are 0.31, 1 and 0.52, respectively.

The homogeneous, isotropic, and constant thermophysical properties of solids were assumed in this study. The contact thermal resistance between solids was disregarded. Grey-diffuse walls were used for radiation modeling. To model the heat transfer for the exterior surfaces including the exterior wall, window and roof, and interior surfaces including interior pipe surface adjacent to flow water, the interior wall of the adjacent room and interior ceiling of adjacent building stories, the boundary conditions of the governing equations are set as Eq. (7).

$$\lambda_{sol} \frac{\partial T}{\partial y}=h_{surf}\left(T_{free}-T_{surf}\right) \quad (7)$$

where λ_{sol} is the solid thermal conductivity of the interior/exterior surface layer, h_{surf} is the convective heat transfer coefficient between the interior/exterior surface and the fluid environment, T_{free} is the free-stream temperature of the surrounding fluid, and T_{surf} is the temperature of interior/exterior surfaces.

The semi-implicit method for pressure-linked equations was adopted for pressure-velocity coupling. The incompressible ideal gas model was used to predict the buoyancy effect. PRESTO! discretization was specified for pressure solution. The radiative heat transfer between indoor surfaces was considered using the discrete ordinates (DO) radiation model [42]. The internal emissivities of the walls, floor, and ceiling were set to 0.9. The second-order discretization scheme was used for the momentum, energy, turbulent kinetic energy, turbulent omega, and discrete ordinates. Convergence was achieved when the residuals were less than 10^{-6} for the energy term and 10^{-4} for all other variables. The thermal resistance of the exterior/interior solid region was taken into account by solving the conjugate heat transfer between the solid region and fluid region in the simulation model. Note that, due to the thermal inertia of the building envelope, the simulation case was first made to reach convergence and run for 24 hours, then the simulated results were analyzed.

2.2.2. Description of the Indoor Conditions

The internal heat gain in the office room was set according to the relevant Chinese design standard [38].

Table **2** presents the occupant, lighting, and equipment heat gains on weekdays. The watts-per-square-meter (W/m^2), which represents the power density, for the 2D building model was calculated by multiplying the floor length and width (1.0 m) in the spanwise direction. A metabolic rate of approximately 1.2 met was considered for predefined occupant body areas (1.45-1.80 m^2) [28] and predefined convective fractions (30%-60%) [28]. Ultimately, a total approximate internal heat load of 185 W (30 W/m^2 for the unit floor area) was accounted for in this office model.

Table 2: Occupant, Equipment, and Lighting Heat Gains on Weekdays [38]

	Value (W/m^2)
Occupant	16
Lighting	9
Equipment	15

Ventilation can remove the latent heat load and provide the minimum outdoor air requirement to ensure the indoor air quality in an office building [43]; therefore, a mechanical air ventilation system must operate in conjunction with a floor heating system. As a commonly used advanced air distribution technique, displacement ventilation is characterized by advantages in improving both the temperature and ventilation effectiveness as compared to other ventilation methods [28, 44, 45].

According to the EN standard 15251 [46], a minimum ventilation airflow rate of 2.1 $l/(s \cdot m^2)$, which is equal to 7.56 $m^3/(h \cdot m^2)$, is recommended. In the Chinese standard GB50189-2015 for office buildings [38], the minimum acceptable outdoor airflow rate is 30 $m^3/(h \cdot person)$. Therefore, both these conditions were considered, and a ventilation rate of 20.5 m^3/h (1.5 ACH) was ultimately used in consideration of the occupant density of 10 m^2/person. A lower ventilation rate is primarily used due to the typical problem of draft risk at the ankle level and the increase of discomfort due to large differences in the vertical air temperature in displacement ventilation systems [47]. Therefore, according to the variant fractions of occupant, equipment, and lighting heat gains at different times, as reported in Table **3**, two constant airflow rates were used, namely 20.5 m^3/h in the periods of 09:00 to 12:00 and 14:00 to 18:00, and 10.25 m^3/h in the remaining working hours.

The range of 14 ^oC to 18 ^oC used for the air supply temperature in the heating season was proven in a previous experiment [24]; thus, the temperature differences between the floor surface and inlet boundary can vary between about 4 ^oC and 14 ^oC, as demonstrated by previously reported measurements [47]. Therefore, regarding the combined floor heating and displacement ventilation system, an air supply temperature with a lower value than the typical design process can reduce the pre-heating period and reduce the energy consumption in a cold climate zone. From this perspective, 16 ^oC was used as the air supply temperature in the present study.

To ensure the airtightness of a building envelope, a constant infiltration rate using the number of air changes per hour (ACH) was used in this study. Infiltration rates in office buildings with minimum ACH values of 0.05 (system-on) [48], 0.1 [49], 0.16 [50], 0.2 [48], 0.2 (system-off) [51], and 0.311 [52] have been extensively measured. Accounting for the airtightness required in an office building, the air-conditioning system-off infiltration rate of 0.2 ACH (2.73 m^3/h) was used in this study, while the system-on infiltration rate was set to zero. In other words, the outdoor air ventilation system was

Table 3: Occupant, Equipment, and Lighting Heat Gains Schedules on Weekdays [38]

Time Slot	Fraction of Occupant Heat Gain	Fraction of Lighting Heat Gain	Fraction of Equipment Heat Gain
00:00-07:00	0.00	0.00	0.00
07:00-08:00	0.10	0.10	0.10
08:00-09:00	0.50	0.50	0.50
09:00-12:00	0.95	0.95	0.95
12:00-14:00	0.80	0.80	0.50
14:00-18:00	0.95	0.95	0.95
18:00-20:00	0.30	0.30	0.30
20:00-24:00	0.00	0.00	0.00

considered to maintain a positive-pressure condition when the system was on.

2.2.3. CFD Boundary Conditions

According to the CFD benchmark test [53-58], the prediction accuracy of CFD simulation depends on the understanding of the fundamentals of fluid dynamics and the setting of appropriate boundary and numerical conditions as well. Moreover, better understandings of a specific simulation problem regarding indoor thermal/pollution environment are also requested. In this study, constant volumetric heat generation rate (q_{source}) was used to model the thermal boundary of the indoor heat source [59], in contrast with the commonly used constant surface temperature and constant surface heat flux methods reviewed by Liu *et al*. [28]. To prevent the effect of an isolated heat source on the local thermal environment, two heat sources with the same volumetric heat generation rate were imposed in the 2D geometry model, as shown in Figure **3**. Two square surfaces with sizes of 0.10×0.10 m were respectively located 1.9 m from the exterior or interior wall and 0.45 m above the heated floor. Correspondingly, the source term for each heat source defined using the calculated q_{source} was set as 10200 W/m^3, e.g., when the fraction was 0.95 during the periods of 09:00-12:00 and 14:00-18:00 according to Table **3**.

Moreover, as given by Eq. (8), a source cover layer with a thickness of 0.01 m was set to indicate the varying thermal conductivity; in other words, when occupants switch off the computers and lights and leave the office, the thermal conductivity of the cover layer (k_{cover}) was considered to decrease substantially (10^{-4}). Additionally, the volumetric heat generation was set to zero, as given by Eq. (9). A user-defined function (UDF) was used in ANSYS FLUENT software to simulate variations of the q_{source} for the occupant, equipment, and lighting heat gains schedules.

$$k_{cover} = \begin{cases} 200, if\ q_{source} \neq 0 \\ 10^{-4}, if\ q_{source} = 0 \end{cases}, \quad (8)$$

$$q_{source} = \sum_{i=1}^{n} \beta_i \cdot q_{i,source}, i = 0 \sim 1, n = 3, \quad (9)$$

where β_i is the fraction of the different heat source types and i indicates the source type.

Interior/exterior convection boundary conditions were set for the inner surface of the pipe and interior/exterior building surfaces using the surface convective heat transfer coefficient and free-stream temperature, as given by Eq. (10).

$$q_{cov} = h_{surf} \cdot (T_{free} - T_{surf}) \quad (10)$$

For a floor heating system, the convective heat transfer coefficient between the inner surface of the pipe and the flowing water (h_{water}) is calculated according to Eq. (11) [60, 61]:

$$h_{water} = \begin{cases} 1.86(Re \cdot Pr)^{1/3} \left(\frac{d}{L}\right)^{1/3} \frac{\lambda_p}{d} \ (\mathrm{Re} \leqq 2300) \\ 0.012(Re^{0.87} - 280) Pr^{0.4} \left(1 + \left(\frac{d}{L}\right)^{2/3}\right) \frac{\lambda_p}{d} (2200 < \mathrm{Re} \leqq 10000) \\ 0.023 Re^{0.8} Pr^{0.3} \frac{\lambda_p}{d} \ (10000 < \mathrm{Re}) \end{cases}, \quad (11)$$

where L is the pipe length (L = 5 m) and d is the pipe radius. In this study, when the water supply velocity was set to 0.5 m/s, h_{water} was approximately 2618 W/(m^2·K) [61]. As this study proposes intermittent control strategies, an on-off control coefficient (β_{CHTC}) was predefined to calculate the realistic heat transfer coefficient (h'_{water}), as given by Eq. (12):

$$h'_{water} = \beta_{CHTC} \cdot h_{water} \quad , \quad (12)$$

where β_{CHTC} is equal to 1 when the system is on; otherwise, it is equal to 0. T_{ave} was set as the free-stream water supply and return temperature that varied with the heating control strategies. It must be noted this average value is a more realistic condition than the water supply temperature, as the pipe length is neglected in the 2D building model. According to the suggestions from the Chinese Standard of Technical Specification for Radiant Heating and Cooling (JGJ142-2012) [62] and the real operating conditions of an office building [63, 64], a maximum T_{ave} value of 35 °C was set.

For the heat gains that transferred through the exterior wall, roof, and window surfaces, the varying outdoor air temperature (T_{out}) was used as the free-stream temperature, and the value of the external surface heat transfer coefficient (h_{ext}) was selected as 25 W/(m^2·K) [65]. Moreover, the surfaces in adjacent office rooms, e.g., the interior walls of adjacent rooms and the ceilings of adjacent building stories, were assumed to have a constant temperature and predefined heat transfer coefficients. The heat transfer coefficients for interior walls (h_{int}) of an adjacent room and the ceiling (h_{ceil}) of the adjacent story were assumed to be 0.948 W/(m^2·K) and 5.0 W/(m^2·K) [66], respectively, and the T_{indoor} representing the indoor air free-stream temperature was set as 18 °C.

The inlet air supply velocity (u_{in}) that accounts for the outdoor air ventilation and infiltration ventilation is defined as follows:

$$u_{in} = \frac{Q_{in}}{A_{in}} = \frac{Q_{in}}{L_{in} \cdot 1.0} = \frac{Q_{in}}{L_{in}}, \quad (13)$$

where Q_{in} is the volumetric airflow rate at the inlet calculated by the outdoor air ventilation rate or infiltration rate (m^3/s), A_{in} is the inlet area (m^2), and L_{in} is the length of the inlet (m). In this study, the calculated inlet velocities for supply air in the working periods between 09:00 to 12:00 and 14:00 to 18:00, and in the remaining working hours (07:00-09:00, 12:00-14:00 and 18:00-20:00), were considered as 0.21 m/s and 0.11 m/s, respectively.

Additionally, the velocity in the infiltration period (unoccupied period) was set as 0.028 m/s. It should be noted that to simplify the geometry model, the infiltration was coming from the DV diffuser when the fan was not used. The CFD boundary conditions are summarized in Table **4**.

2.2.4. Computational Grid Distribution

Hybrid meshes were used, including triangular meshes around the heating pipe and quadrilateral meshes in other solid zones and the indoor air zone. The thickness of the first layer with a 1.2 growth rate adjacent to the heat source and heated floor was made very small (0.4 mm) to resolve the laminar sublayer, where the non-dimensional wall distance (y^+) was less than 1. The grid sizes of the inlet and outlet openings were 5 mm with total numbers of 8 cells, respectively. Also, each component in the multilayer structures maintained at least 3 cells in the heat transfer direction from the inside to outside.

To ensure the quality control of CFD simulation [58, 67], a grid independence analysis was conducted by adjusting the element sizes of the heating pipe and heat source. As shown in Table **5**, the heated floor temperature and indoor air temperature at a height of 1.1 m were compared. The relative differences between two adjacent grid distributions under the stipulated parameters were very small (<1%) due to the rigorous boundary layer distribution and the sufficient number of cells, e.g., inlet and outlet, predefined in advance. According to the maximum relative differences of the floor surface temperature and air temperature at the height of 1.1 m, 291,772 cells in total were ultimately used for all further simulation cases. Figure **5** presents the grid distributions specifically around the heat source, the heated floor, and the heating pipe. Moreover, the time step of 15 s was considered after taking into account the tradeoff between computational resources and simulation accuracy [35].

Table 4: A Summary of the CFD Boundary Conditions

	07:00-20:00 on Weekdays	Other Times on Weekdays
Inlet	Uniform u_{in} (0.21 m/s or 0.11 m/s), constant T_{in} (16 °C)	Uniform u_{in} (0.028 m/s), variable T_{in}
Outlet	Pressure out	Pressure out
Pipe wall	T_{ave} and h'_{water} varied with the control strategies	T_{ave} and h'_{water} varied with the control strategies
Heat sources	q_{source} varied with the schedules	0
Exterior roof	Variable T_{out}, constant h_{ext}	Variable T_{out}, constant h_{ext}
Exterior wall	Variable T_{out}, constant h_{ext}	Variable T_{out}, constant h_{ext}
Exterior window	Variable T_{out}, constant h_{ext}	Variable T_{out}, constant h_{ext}
Interior walls of adjacent room	Constant T_{indoor} and h_{int}	Constant T_{indoor} and h_{int}
Ceiling of adjacent building story	Constant T_{indoor} and h_{ceil}	Constant T_{indoor} and h_{ceil}

Table 5: Grid Independence Analysis

	Pipe Element Size/Heat Source Grid Size	Total Number of Grids	Relative Difference of Floor Surface Temperature	Relative Difference of Air Temperature at a Height of 1.1 m
Coarse mesh	1.5 mm/15 m	198,676	-	-
Medium mesh	1 mm/10 mm	291,772	0.73%	0.94%
Fine mesh	0.8 mm/8 mm	344,672	0.26%	0.51%

Note: The boundary layers around the heat source, the grid numbers (≥8) of the inlet and outlet, and the grid number (≥3) for each component in the multilayer structures were kept constant for each case.

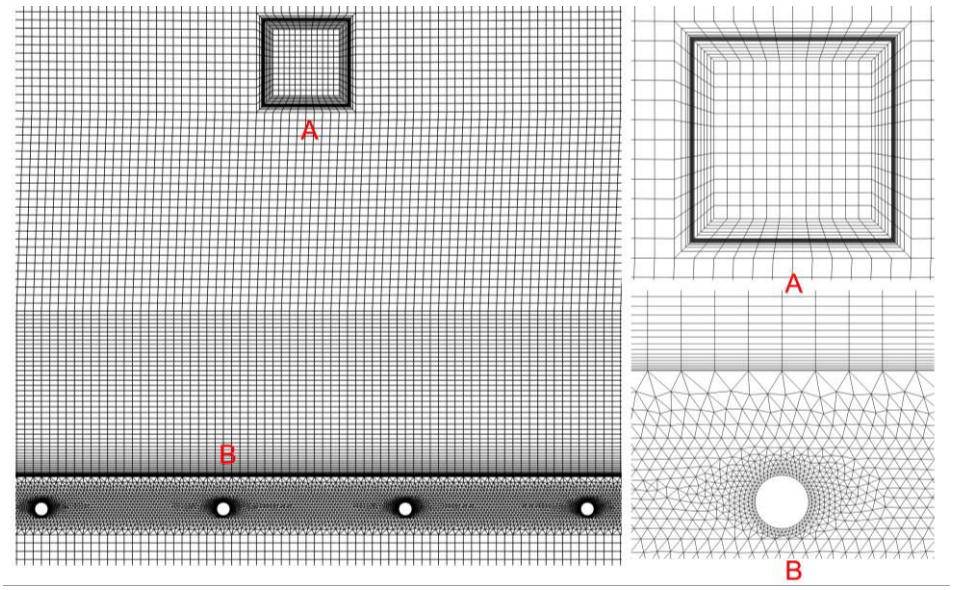

Figure 5: Grid distributions of the 2D simulation model around the heat source at section A, and the heated floor and heating pipe at section B.

2.3. Control Strategy and Meteorological Data

2.3.1. Meteorological Data

Numerical simulation was conducted under the weather conditions in Jinan, China, which is located in a cold climate zone. The daily temperature profile and solar radiation variation were sourced from the Chinese Standard Weather Database adopted in the EnergyPlus simulation program [68]. Proposed daily weather conditions including between December 11 and December 21 were then created, as shown in Figure **6**. The maximum and minimum T_{out} values were 4.3 °C at 15:00 and -4.2 °C at 05:00. The maximum direct solar radiation (Q_{dir}) was set to two different values of 736 and 446 W/m^2 at 13:00. The maximum daily temperature difference was about 8.5 °C. It should be noted that this daily temperature variation profile was used for the subsequent control strategies. In other words, the daily temperature difference was kept constant, while temperature profiles varied depending on $T_{min,out}$.

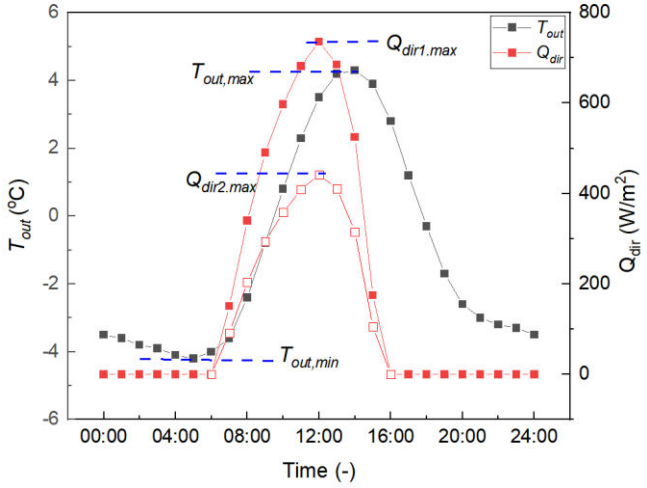

Figure 6: The variations of predefined T_{out} and Q_{dir} (The blue dash lines indicate the minimum or maximum T_{out} and Q_{dir}).

2.3.2. Control Strategy

An intermittently-operated heating strategy using T_{ave} based on different $T_{min,out}$ values is proposed according to existing studies [19, 69], as given by Eqs. (14-18).

If $T_{min,out}$ ≤ -15 °C, then

$$T_{ave} = T_{water,high} \tag{14}$$

If -15 °C < $T_{min,out}$ ≤ 15 °C, then

$$\alpha_{min,out} = \frac{T_{water,low} - T_{water,high}}{T_{out,high} - T_{out,low}} \tag{15}$$

$$T_i = (T_{water,high} + T_{water,low})/2 \tag{16}$$

$$T_{ave} = \alpha_{min,out} \cdot T_{min,out} + T_i \tag{17}$$

If $T_{min,out}$ > 15 °C, then

$$T_{ave} = T_{water,low} \tag{18}$$

In In Eqs. (14-18), $T_{water,low}$ is the lowest set-point temperature for the average water temperature (25 °C in this study), $T_{water,high}$ is the highest set-point temperature for the average water temperature (35 °C in this study),

$T_{out,low}$ is the predefined lowest value of T_{out} (-15 °C in this study), $T_{out,high}$ is the predefined highest value of T_{out} (15 °C in this study), $\alpha_{min,out}$ is the slope of the control method, and T_i is the average reference temperature. Figure **7** presents the control strategies for setting a predefined water supply and return temperature with the variation of $T_{min,out}$.

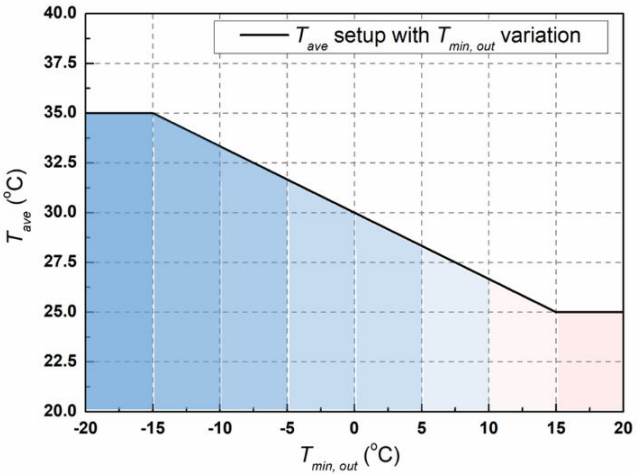

Figure 7: Proposed control strategies for setting the T_{ave} as a function of $T_{min,out}$.

In this study, different intermittent operation cases were defined and the indoor thermal comfort condition was evaluated according to the proposed control strategies using the numerical method. As reported in Table **6**, six different $T_{min,out}$ values in different climatic control zones were selected, and T_{ave} was accordingly defined. Note that this study excluded the extreme cold and extreme warm climatic conditions with $T_{min,out} \leq$ -15 °C or $T_{min,out} >$ 15 °C during the heating season in Jinan city. In fact, a continuous operation should be carried out in the climatic zone of $T_{min,out} \leq$ -15 °C, and a non-operational heating system may be considered in the climatic zone of $T_{min,out} >$ 15 °C.

Table 6: Case Descriptions for Average Water Set-Point Temperatures Selected Under Different Outdoor Climatic Conditions

Climatic Control Zone	Assumed $T_{min,out}$ (°C)	T_{ave} (°C)
-15 °C < $T_{min,out}$ ≤ -10 °C	-14.2	34.7
-10 °C < $T_{min,out}$ ≤ -5 °C	-9.2	33.1
-5 °C < $T_{min,out}$ ≤ 0 °C	-4.2	31.4
0 °C < $T_{min,out}$ ≤ 5 °C	0.8	29.7
5 °C < $T_{min,out}$ ≤ 10 °C	5.8	28.1
10 °C < $T_{min,out}$ ≤ 15 °C	10.8	26.4

Considering the schedules of the occupancy, equipment heat gain, and lighting heat gain in the office building, intermittent operation strategies for noon and nighttime are proposed. Figure **8** presents the values of T_{ave} and the schedules under different conditions of T_{out}. For example, in Case T-14.2, when the forecast daily minimum temperature was between -15 °C and -10 °C (-14.2 °C), as recommended in Figure (**8a**), the heating water was supplied to the floor in three different periods, namely 00:00-11:00 and 13:00-18:00 (total 16 hours), 00:00-11:00 and 13:00-20:00 (total 18 hours), and 00:00-11:00 and 13:00-22:00 (total 20 hours).

As the outdoor air temperature increases, the values of T_{ave} and the operation schedules decrease differently. Numerical simulations were conducted to compare the indoor thermal comfort environment in different intermittently-operated cases. By comparing the results, the final floor heating system control strategies were obtained.

2.3.3. The Effect of Solar Radiation

Existing revealed that the heat gains of exterior surfaces from direct solar radiation and the heat gains of floor surfaces from the incident sunlight transmitted through windows had significant effects on the radiant floor performance [70,71]. The solar radiation beneficially decreases the power demand of radiant floor heating systems [72]. Considering the purpose of this study, only the heat gains through exterior surfaces (window, walls, and roof) were considered. The modified control strategies only focus on reducing the floor heating period or increasing the intermittent period, especially at noon.

For the external surfaces affected by direct solar radiation, the sol-air temperature ($T_{sol-air}$) is used as a variable to determine the total heat gain transferred through exterior surfaces, as given by Eq. (19) [73]:

$$T_{sol-air} = T_{out} + \frac{a \cdot I}{h_{out}} - \frac{Q_{lw}}{h_{out}} \quad (19)$$

where *a i*s the solar radiation absorptivity (0.8 in this study), h_{out} is the heat transfer coefficient of the external surfaces (25 W/(m^2·K), I is the total solar radiation incident on the surface, Q_{lw} is extra infrared radiation due to the difference between the external air temperature and the apparent sky temperature.

In this study, the effect of longwave radiation, e.g., that at night, was neglected. Table **7** describes case studies of modified control strategies under the exterior climatic condition of -15 °C < $T_{min,out}$ ≤ -10 °C. As for the

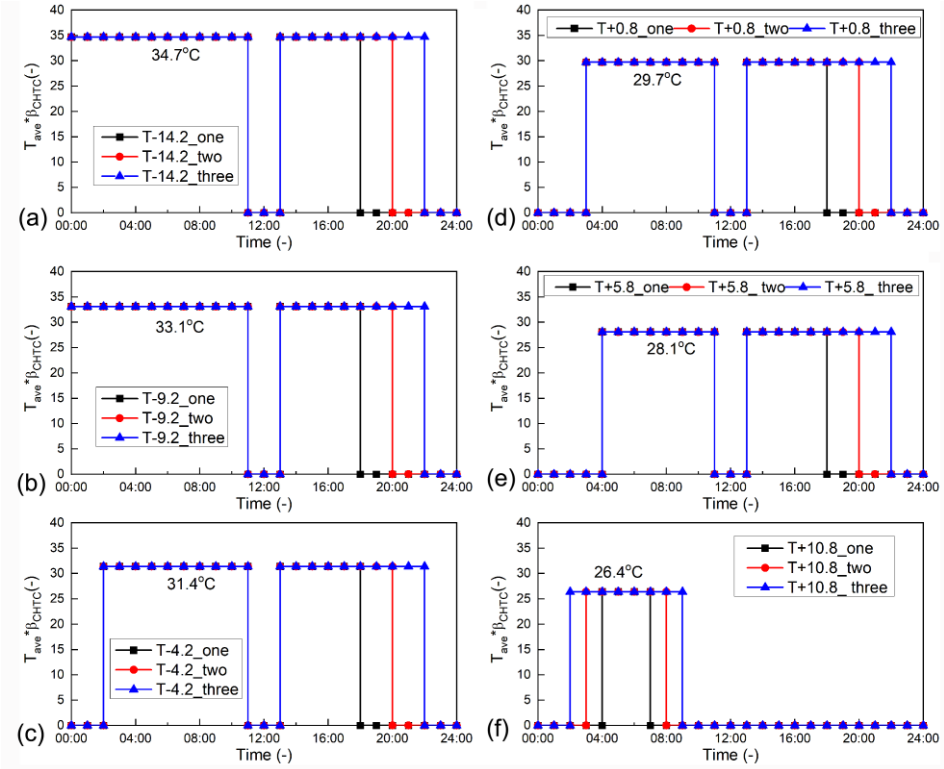

Figure 8: Water supply schedules (T_{ave}*β) under different T_{out} conditions: (a) $T_{min,out1}$ = -14.2 °C; (b) $T_{min,out2}$ = -9.2 °C; (c) $T_{min,out3}$ = -4.2 °C; (d) $T_{min,out4}$ = 0.8 °C; (e) $T_{min,out5}$ = 5.8 °C; (f) $T_{min,out6}$ = 10.8 °C.

air supply and infiltration boundary conditions, the inlet velocities were set as 0.21m/s in the periods between 09:00 to 12:00 and 14:00 to 18:00, and 0.11m/s in the remaining working hours (07:00-09:00, 12:00-14:00 and 18:00-20:00). Moreover, the infiltration air velocity was set as 0.028m/s.

Table 7: Modified Control Strategies Under the Exterior Climatic Conditions of -15 °C < $T_{min,out}$ ≤ -10 °C

	Maximum Q_{dir} (W/m^2)	Heating Schedule	T_{ave}(°C)
Case sol0*	0	00:00-11:00, 13:00-20:00	34.7
Case sol1	446	00:00-11:00, 13:00-20:00	34.7
Case sol2	736	00:00-11:00, 14:00-20:00	34.7

Note: Case sol0* indicates the absence of the solar radiation effect.

2.4. Thermal Comfort Evaluation Criteria

To provide an acceptable indoor thermal environment with the radiant floor heating system, the requirements for general thermal comfort, e.g., the Predicted Mean Vote (PMV), Predicted Percentage of Dissatisfied (PPD), and operative temperature (T_{op}), as well as the local thermal comfort criteria, e.g., the vertical air temperature differences between the head and ankles ($\Delta T_{0.1-1.1}$), floor heating temperature (T_{fl}), radiant asymmetry (ΔT_{pr}) [74], and draft risk (DR), should be taken into account [75].

This study mainly focused on the local thermal comfort indices, and the PMV and PPD were not considered due to the required assumption of certain parameters, including the air humidity, occupant clothing insulation, and occupant metabolic rate. Therefore, the operative temperature, vertical air temperature difference, floor temperature, and radiant asymmetry were used as the thermal comfort criteria. Moreover, the percentages dissatisfied (PD) due to vertical air temperature differences ($PD_{\Delta T0.1-1.1}$), a warm floor temperature (PD_{Tfl}), and radiant asymmetry ($PD_{\Delta Tpr}$), e.g., cool walls, were respectively employed.

Regarding the operative temperature defined in Eq. (20), the mean radiative temperature and air temperature in the occupied zone are used to account for the convective heat transfer coefficient and radiative heat transfer coefficient. Here, the operative temperate is calculated as the adjusted air temperature, as given by Eq. (21).

$$T_{op} = \frac{h_c T_a + h_r T_{mrt}}{h_c + h_r} \quad (20)$$

$$T_{op} \approx T_{adjust} = \frac{T_a + T_{mrt}}{2} \quad (21)$$

$$T_{mrt} = \sqrt[4]{\sum_{j=1}^{n}(F_{p-j}T_j^4)} \quad (22)$$

$$T_{mrt} = \frac{0.18\cdot(T_{pr,up}+T_{pr,down})+0.22\cdot(T_{pr,left}+T_{pr,right})+0.30\cdot(T_{pr,front}+T_{pr,back})}{2\cdot(0.18+0.22+0.30)} \quad (23)$$

$$T_{mrt} = 0.13 \cdot \left(T_{pr,up} + T_{pr,down}\right) + 0.185 \cdot \left(T_{pr,left} + 3 \cdot T_{pr,right}\right) \quad (24)$$

The mean radiant temperature (T_{mrt}) is then calculated using the view factors between the body of a sitting occupant and room surfaces according to Eq. (22). As shown in Eq. (23), an evaluation method of the mean radiant temperature provided by the EN ISO standard 7730 is used [36]. Due to a lack of front and back surfaces in the 2D model, the radiant temperatures of these two surfaces are calculated using that of the surface located to the left side of the occupant (the interior wall in the CFD model). Finally, the mean radiant temperature is calculated according to Eq. (24) [76].

The PD due to differences in the vertical air temperature at the head and ankle levels is calculated according to Eq. (25) based on the EN ISO standard 7730 [36].

$$PD_{\Delta T0.1-1.1} = \frac{100}{1+\exp(5.76-0.856\cdot\Delta T_{0.1-1.1})} \quad (25)$$

The PD due to a warm floor in the floor heating system is calculated by Eq. (26) using the equation given in the ISO standard 7730 [36].

$$PD_{Tfl} = 100 - 94 \cdot \exp(-1.387 + 0.118T_{fl} - 0.0025 \cdot T_{fl}^2) \quad (26)$$

The difference of surface radiant temperatures between the left side (exterior window and wall) and right side (interior wall) of the 2D model are used to calculate the ΔT_{pr} in the horizontal direction. Correspondingly, the equation for PD presented in the EN ISO standard 7730 that considers the radiant asymmetry in the floor heating system is given by Eq. (27) [36].

$$PD_{\Delta Tpr} = \frac{100}{1+\exp(6.61-0.345\cdot\Delta T_{pr})} \quad (27)$$

The thermal comfort criteria according to the EN ISO standard 7730 [36] and ASHRAE standard 55 [77] defined using the operative temperature in the heating period are provided in Table **4**. In this study, category B, which represents 90% of thermally satisfied occupants, was taken into account. The thermal comfort limits for the values of $\Delta T_{0.1-1.1}$, T_{fl}, and ΔT_{pr}, as well as the PDs affected by these parameters, are also presented in Table **8**.

2.5. CFD Simulation Validation

The CFD simulation validations were conducted to compare the radiation heat transfer and air distribution in a 2D building model (with a heat source) and to analyze the floor heating performance of an intermittently-operated system emended with a water pipe. The CFD simulation validation was divided into two parts: (1) the validation of thermal radiation on airflow with displacement ventilation in the 2D model; (2) the validation of the intermittent period of the floor heating system with the heat-releasing process in the 2D model.

An experiment of a ventilated cavity for indoor ventilation was conducted by Blay *et al*. [78], in which cold air was injected from an inlet at the upper-left side of a cavity and exhausted from an outlet at the lower-right side. A floor surface was heated at a constant temperature. Figure **9** presents the configuration of the 2D simulation of the ventilated cavity experiment. It should be noted that the original cavity model was 3D with a size of 1.04×0.3×1.04 m (*L*×*W*×*H*) with an inlet opening size of 1.01×0.018 m and an outlet opening size of 1.04×0.024 m. Note that the widths of

Table 8: Thermal Comfort Criteria in the Heating Period According to the EN ISO Standard 7730 [36] and ASHRAE Standard 55 [77]

	EN ISO Standard 7730					ASHRAE Standard 55	
	Category A		Category B			Category A	Category B
	Condition	PD (%)	Condition	PD (%)		Condition	Condition
T_{fl}	19-29 °C	≤10	19-29 °C	≤10	T_{op}	21-23 °C	20-24 °C
$\Delta T_{0.1-1.1}$	<2 °C	≤3	<3 °C	≤5			
ΔT_{pr}	<10 °C	≤5	<10 °C	≤5			

the inlet and outlet were the same (0.3 m); therefore, the effect of heat transfer on the spanwise side was neglected in the present simulation.

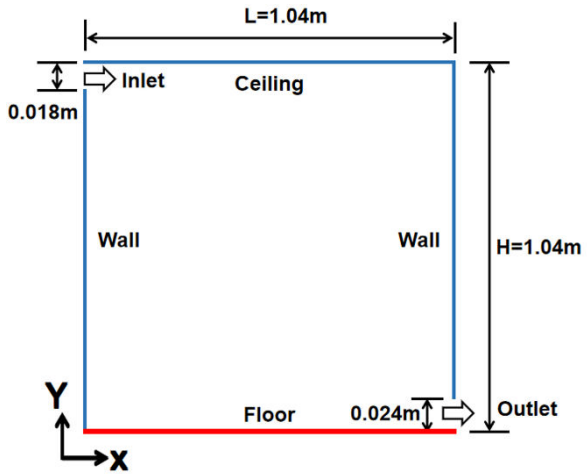

Figure 9: Configuration of a 2D simulation model of a ventilated cavity experiment [78].

The floor wall was set as having a constant temperature of 35 °C, and all other surfaces had the same temperature of 15 °C. The inlet velocity was set as 0.57 m/s with a temperature of 15 °C, representing the Reynolds number of 684 and the Rayleigh number of 2.6×10^9 based on the inlet boundary condition. The turbulent intensity and turbulent length were set as 5% and 0.015, respectively. A good grid resolution of 120×120 in the 2D model was used, resulting in a small value of y^+ (≈1) adjacent to the wall surface.

The comparisons between the simulated results and measured data are presented in Figure **10**, in which the air temperature profiles in the centerline x/X = 0.5 and y/Y = 0.5, and the velocity profiles for component *u* in x/X = 0.5 and component *w* in y/Y = 0.5, are compared. The figures indicate a good agreement between the air temperature near the surfaces in the center zone of the room, and an acceptable discrepancy of about 2.5% between the simulated and measured results was observed. With regard to the *u* and *w* velocities, a clockwise-rotating vortex occurred in the cavity, resulting in larger velocity magnitudes adjacent to the cavity surfaces with a fairly small difference from the experimental data. In summary, the numerical model is capable of accurately capturing the flow vortex and predicting the variation of the air temperature in the cavity zone. The overall performance of the CFD simulation is therefore acceptable.

A field experiment for an intermittently-operated floor heating system was conducted in a test building, based on which the numerical model in the present study was constructed, as shown in Figure **2**. In the field study [79], the indoor air temperatures at different heights (0.1 m,

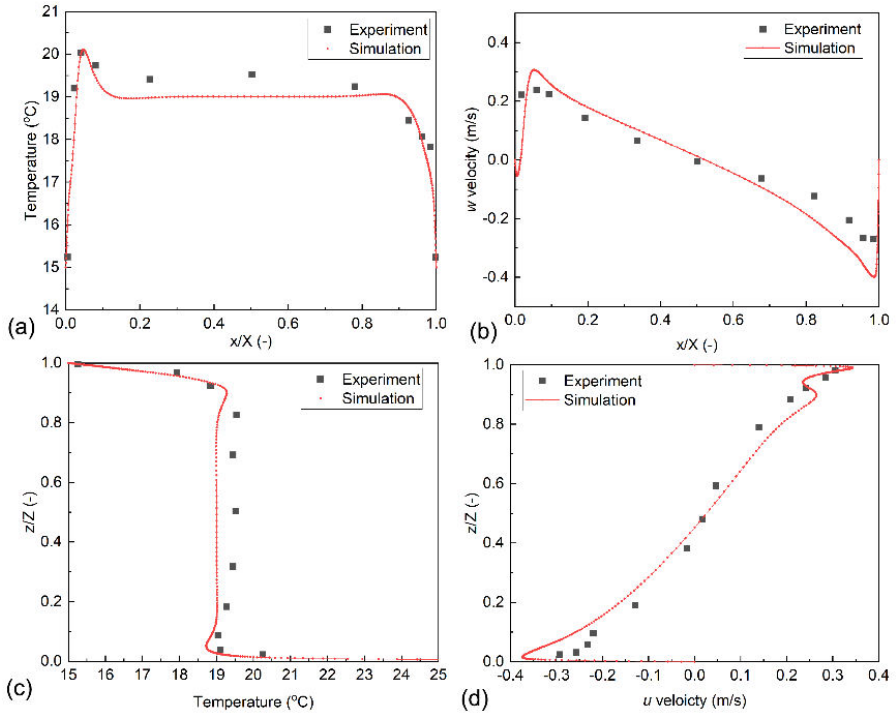

Figure 10: Comparisons between simulated results and measured data: (a) Air temperature in y/Y = 0.5; (b) *w* velocity in y/Y = 0.5; (c) air temperature in x/X = 0.5; (d) *u* velocity in x/X = 0.5.

0.6 m, 1.1 m, 1.7 m, and 2.3 m) were measured using DS1922L iButton sensors with an accuracy of ±0.5 °C, as depicted in Figure **11**.

The interior walls and floor temperature were measured using a multi-channel temperature acquisition instrument and validated with a FOTRIC 220s infrared thermal camera with an accuracy of ±2%. T_{ave} was also monitored to ensure the correct on-off time of the heating period. Moreover, T_{out} and the direct solar radiation from 12:00 on December 31, 2015, to 09:00 on January 1, 2016, were measured using a weather station at the rooftop of the building, as presented in Figure **12**. The water supply was shut off at 17:00 on December 31, 2015. The value of T_{ave} was set as approximately 24.5 °C starting from 12:00 at noon.

Figure 11: The locations of the iButton temperature sensors in test room study.

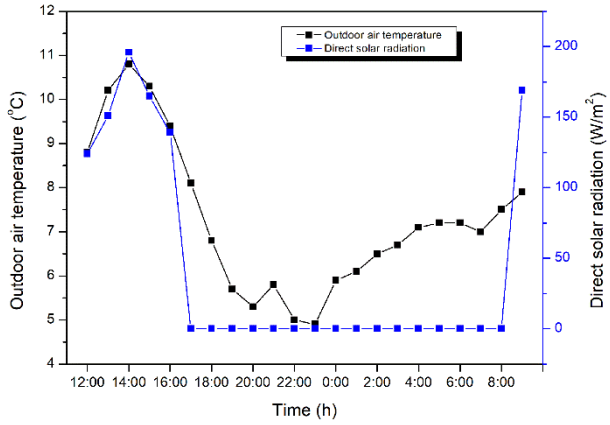

Figure 12: The variation of T_{out} and Q_{dir} in the horizontal surface from 12:00 on December 31, 2015 to 09:00 on January 1, 2016.

This validation study only considered the heat release process from 12:00 on December 31, 2015, to 09:00 on January 1, 2016, the period of the New Year holiday. To prevent the effects of indoor heat gains, no occupants stayed in the office, and the equipment and lighting were shut off starting from 12:00 on December 31, 2015. Therefore, to study the transient thermal environment in the floor heating system of the building envelope, the variations of the indoor air temperature and floor surface temperature in the study period were compared, as shown in Figures **13** and **14**. Due to the thermal inertia of the building envelope, the simulation case reached steady-state conditions and was run for 24 hours before the actual simulation period.

As shown in Figure **13**, the variations of the indoor air temperature at different heights exhibit smoothly decreasing curves. Both the measurement and simulation data present a remarkable stratification in the vertical direction. The comparison reveals that the simulation study experienced a slightly slower heat release process when the water supply was shut off, and a faster heat release process 5 hours after the pump was shut off. The maximum air temperature difference at different heights (0.1 m, 1.1 m, and 2.3 m) reached about 0.35 °C, 0.42 °C, and 0.3 °C, respectively. The figure indicates a good agreement for the indoor air temperature with a relatively acceptable discrepancy of up to 2.6%. Moreover, as revealed by the surface temperature variations presented in Figure **14**, a maximum temperature of 0.5 °C between the simulation and measurement data was observed. Ultimately, the overall performance of the transient CFD simulation for a floor heating system with a heat release process is acceptable.

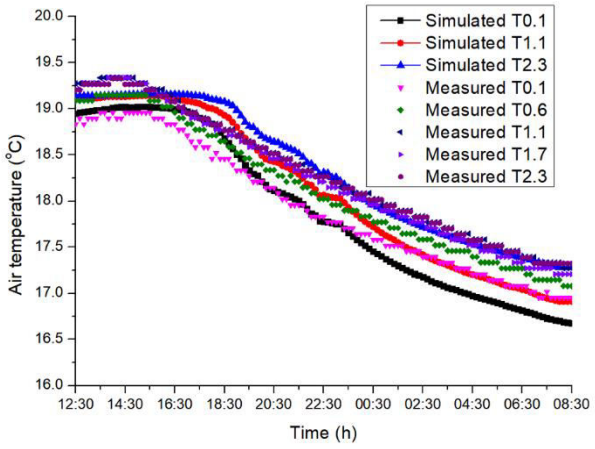

Figure 13: Simulated and measured indoor air temperature from 12:00 on December 31, 2015 to 09:00 on January 1, 2016.

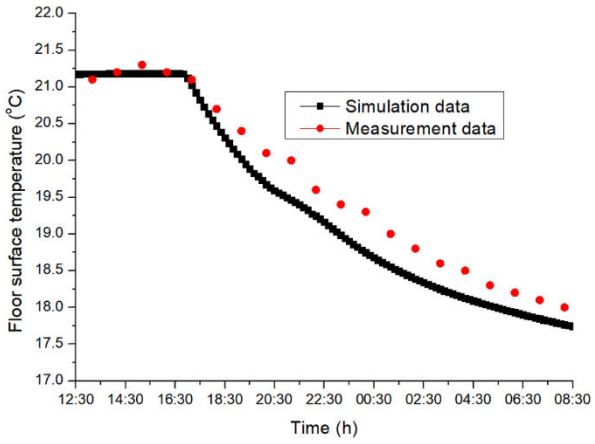

Figure 14: Simulated and measured average floor temperatures from 12:30 on December 31, 2015 to 08:30 am on January 1, 2016.

3. RESULTS

The results present the indoor air velocity and air temperature distributions for an example case in which $T_{min,out}$ = -14.2 °C. The operative temperature and the PDs due to T_{fl}, $\Delta T_{0.1-1.1}$, and ΔT_{pr} are compared. Finally, the effect of solar radiation on the temperature variation of interior surfaces, including the windows, ceiling, and walls, is analyzed when $T_{min,out}$ = -14.2 °C.

3.1. Air Velocity and Air Temperature Distribution

To compare the performances of different control strategies based on T_{ave} and the schedules, the contour distributions of the air velocity and air temperature are presented. The case in which $T_{min,out}$ = -14.2 °C is taken as an example with three different water supply schedules, namely 00:00-11:00 and 13:00-18:00 (Case T-14.2_one), 00:00-11:00 and 13:00-20:00 (Case T-14.2_two), and 00:00-11:00 and 13:00-22:00 (Case T-14.2_three). The air velocity and air temperature at the two times of 07:00 in the morning and 14:00 at noon are presented.

Figure **15** presents the contour distributions of the air velocity and temperature at 07:00 for Case T-14.2. The figure reveals the obvious downdraft from cold surfaces (walls and windows) when the infiltration air coming from the inlet spreads across the floor. Although the inlet

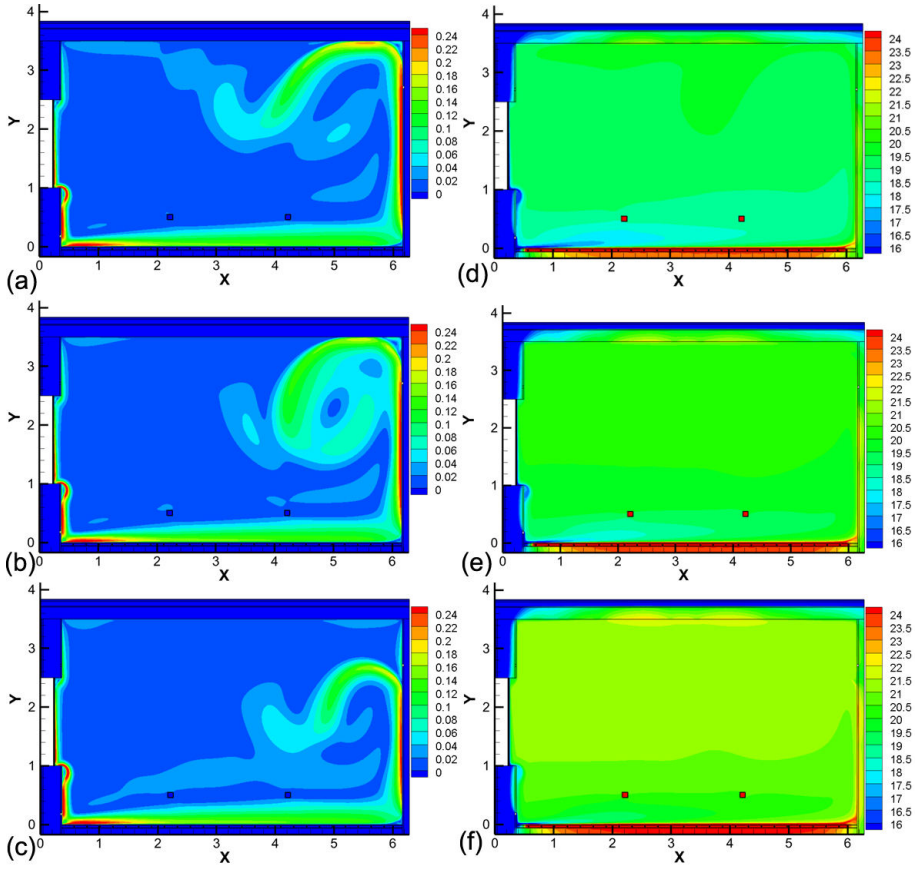

Figure 15: Contour distributions of air velocity and temperature at 07:00 for Case T-14.2: (a) velocity for Case T-14.2_one; (b) velocity for Case T-14.2_two; (c) velocity for Case T-14.2_three; (d) temperature for Case T-14.2_one; (e) temperature for Case T-14.2_two; (f) temperature for Case T-14.2_three.

velocity with an infiltration rate of 0.2 ACH was only 0.028 m/s, the velocity adjacent to the floor reached about 0.24 m/s due to the combined effect of thermal plumes and jet.

Regarding the air velocity, there was no significant discrepancy among the cases in which the water supply was shut off at 18:00, 20:00, and 22:00 in those three cases, except for the locations at the top-right corner. This may be explained by the presence of a larger stratification, especially the higher temperature near the ceiling. The higher the temperature near the ceiling, the more difficult it is for the cold air to blow across the vertical wall to the ceiling. The average air temperature at the heights of 0.1 m and 3.0 m ranged from about 17.9 ^{o}C to 20.2 ^{o}C for Case T-14.2_one, from about 18.8 ^{o}C to 20.6 ^{o}C for Case T-14.2_two, and from about 20.1 ^{o}C to 21.8 ^{o}C for Case T-14.2_three. Therefore, from this perspective, the earlier shut-off of the water supply may not contribute to maintaining a comfortable environment at 07:00.

Figure **16** depicts the contour distributions of the air velocity and temperature at 14:00 for Case T-14.2. A remarkable thermal plume flow around the heat source with the maximum velocity magnitude of about 0.3 m/s was observed. Due to the complex effects of the heat source buoyancy and inlet flow in the 2D section, the indoor airflow presented some irregular recirculation. Correspondingly, the indoor air temperature distribution reveals unobvious thermal stratification, especially at the top zone, as compared with the case at the time of 07:00.

However, the vertical air temperature differences for the three cases remained roughly between 0.8 ^{o}C and 1.1 ^{o}C due to the effect of the slightly higher-temperature buoyancy flow in the zone at the height of 1.1 m. Moreover, the overall average indoor air temperature reached about 25.0 ^{o}C when the water supply was shut off later, as compared with about 23.0 ^{o}C when the water supply was shut off earlier. Therefore, suitable on-off control strategies are necessary to maintain an

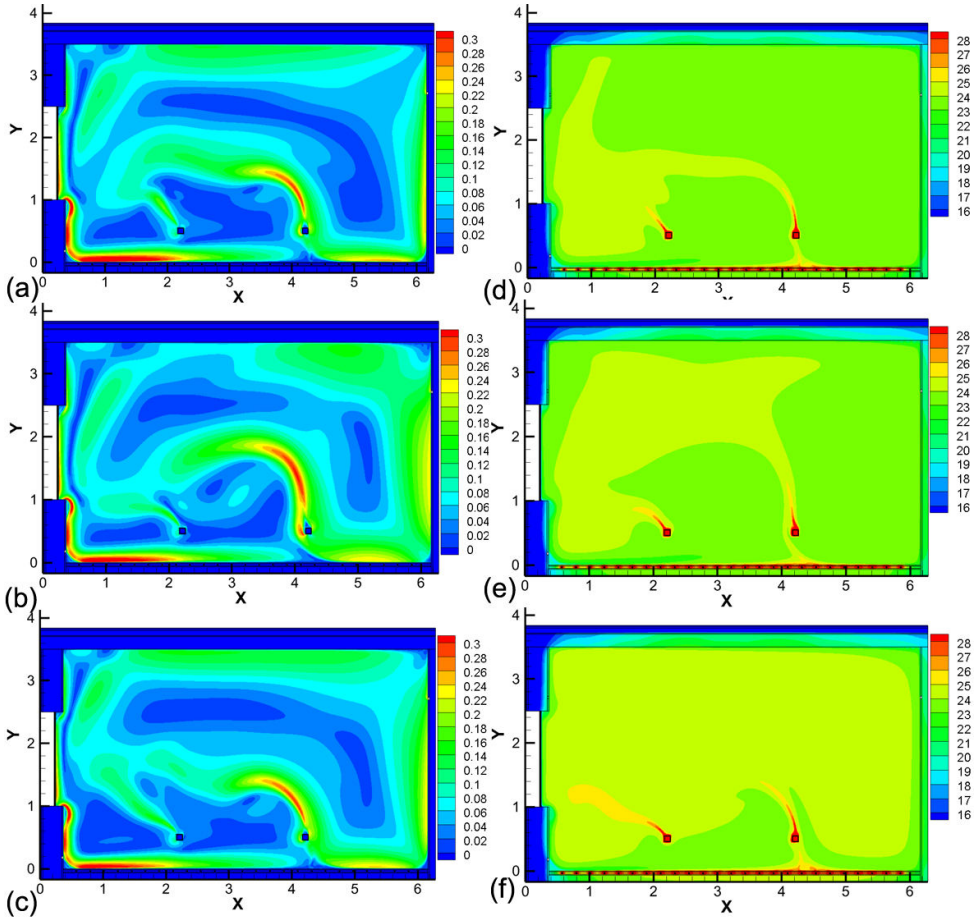

Figure 16: Contour distributions of air velocity and temperature at 14:00 for Case T-14.2: (a) velocity for Case T-14.2_one; (b) velocity for Case T-14.2_two; (c) velocity for Case T-14.2_three; (d) temperature for Case T-14.2_one; (e) temperature for Case T-14.2_two; (f) temperature for Case T-14.2_three.

acceptable thermal comfort environment while preventing a too-warm thermal environment.

To analyze the variations of the indoor thermal environment with the heat gains and the switching on and off of the water supply, Figure **17** presents the hourly variations of the average indoor air temperature at 1.1m level ($T_{1.1}$) under all six $T_{min,out}$ conditions and the corresponding control strategies as shown in Figure **8**. All the control strategies can maintain a certain indoor air temperature above 18 °C at the height of 1.1 m, even when T_{out} is as low as -14.2 °C at 05:00. However, due to thermal stratification, the operative temperature and more thermal comfort indices must be comprehensively analyzed to determine whether the thermal comfort environment is acceptable.

Figure **17** also demonstrates that the indoor heat gain had a significant effect on the indoor air temperature; for example, when people occupied the office from 07:00-08:00 and 08:00-09:00 with respective equipment and lighting fractions of 0.1 and 0.5, the indoor air temperature gradually increased. Note that the temperature rise was obvious beginning at 07:00, which is attributed to the assumption of a step change for the indoor heat gain instead of a continuous change. Further studies may consider more realistic conditions. When the indoor heat gain gradually disappeared starting at 18:00, the indoor air temperature gradually decreased. The decrement of the air temperature reached about 4.0 °C for Case T-14.2 and 1.0 °C for Case T+10.8. In addition to the effect of heat transfer through the building envelope from a slightly lower T_{out}, the assumed infiltration ventilation played a significant role.

For cases with an obvious increase of air temperature starting at noon (12:00-14:00), especially Case T+5.8 and Case T+10.8, this was mainly due to the decrease of the air supply volume with a relatively lower temperature. In summary, the hourly variations of the indoor air temperature remarkably indicate the relatively realistic changes of the indoor thermal environment based on the different control strategies.

3.2. Evaluation of the Operative Temperature

Figure **18** presents the split heatmaps of the indoor operative temperature with different control strategies. As defined by the thermal comfort criteria during the heating period presented in Table **8**, only the range of 20 °C to 24 °C is exhibited in the split heatmaps. As it could be expected, the control strategies could not maintain the operative temperature above 20 °C throughout the day when the water supply was shut off at an earlier time (18:00). The maximum operative temperature commonly occurred in the afternoon between 16:00-18:00, which can be explained by the raised mean radiant temperature. In other words, the increasing temperature of the interior surfaces of the building envelope affected the mean radiant temperature by storing heat during the daytime.

For the case $T_{min,out}$ = -14.2 °C, when the water supply was shut off at 18:00, the operative temperature at 07:00 had a lower value of about 19.8 °C and gradually increased when occupants arrived and started to use the equipment and lighting. When the water supply was shut off after 20:00 and the pump was started to recirculate water in the concrete slab at 00:00, an acceptable temperature at 07:00 was guaranteed. For the case $T_{min,out}$ = -9.2 °C, the T_{ave} value of 33.1 °C maintained a better environment regardless of whether the water supply was shut off at 18:00 or 20:00. Therefore, an intermittently-operated case with the water supply shut off for 6 hours from 18:00-00:00 and

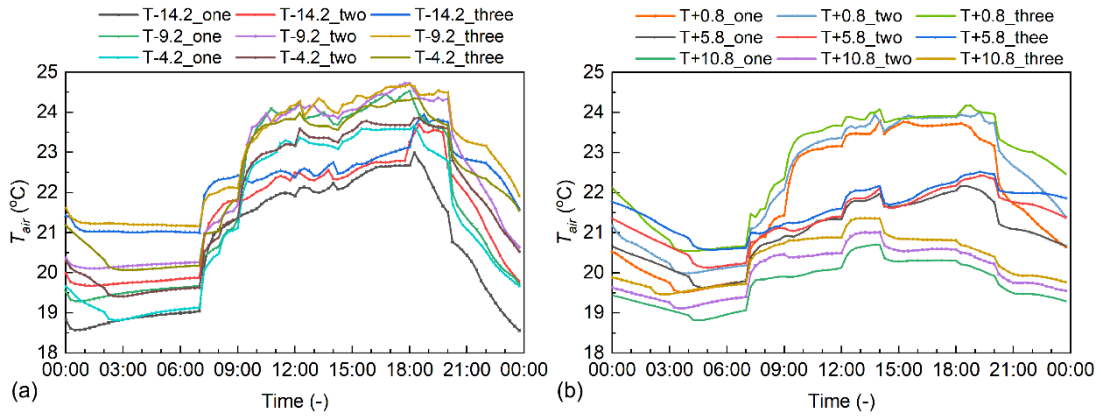

Figure 17: Hourly variation of indoor air average temperature ($T_{1.1}$) with different control strategies: (a) $T_{min,out1}$ = -14.2 °C; (b) $T_{min,out2}$ = -9.2 °C; (c) $T_{min,out3}$ = -4.2 °C; (d) $T_{min,out4}$ = 0.8 °C; (e) $T_{min,out5}$ = 5.8 °C; (f) $T_{min,out6}$ = 10.8 °C.

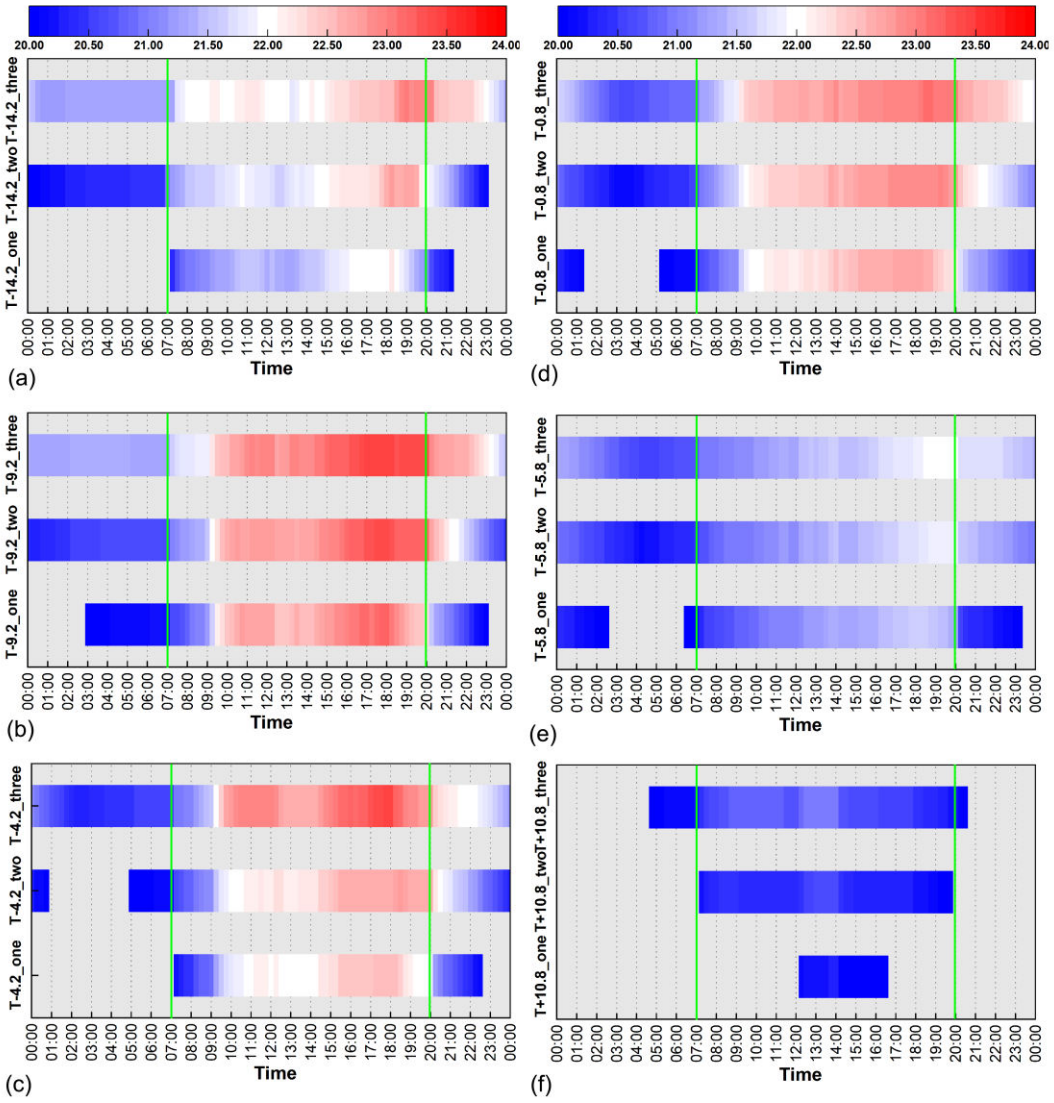

Figure 18: Split heatmaps for the operative temperature with six different control strategies: (a) $T_{min,out1}$ = -14.2 °C; (b) $T_{min,out2}$ = -9.2 °C; (c) $T_{min,out3}$ = -4.2°C; (d) $T_{min,out4}$ = 0.8 °C; (e) $T_{min,out5}$ = 5.8 °C; (f) $T_{min,out6}$ = 10.8 °C.

for 2 hours from 12:00-14:00 presents a good performance and has a good energy-saving characteristic.

For the case $T_{min,out}$ = -4.2 °C, the performance was the same as that of the case $T_{min,out}$ = -14.2 °C. A reliable solution is a later shut-off of the water supply, e.g., at 20:00, and an earlier opening of the water supply at 02:00. As discussed in the previous section, the indoor heat gain appeared, resulting in a significant amount of heat, which benefitted the radiant floor heating system. Therefore, to eliminate the effect of the indoor heat gain, a water supply shut-off after 20:00 is encouraged in the case of an insufficient indoor heat gain during the next daytime.

For the cases of $T_{min,out}$ = 0.8 °C and $T_{min,out}$ = 5.8 °C, it is acceptable to consider shutting off the water supply after 18:00 and turning on the water pump after 03:00 or 04:00. Correspondingly, a daily period with up to 10 hours without a heating water supply can still maintain a relatively acceptable environment. For the case $T_{min,out}$ = 10.8 °C, a T_{ave} value of 26.4 °C when the water supply period ranged from 02:00 to 09:00 was found to result in a good performance. Ultimately, different control strategies were demonstrated according to different values of $T_{min,out}$.

3.3. Evaluation of Local Thermal Comfort

According to the EN ISO standard 7730 [36] for the thermal comfort criteria, the category B conditions were used in this study, including T_{fl} (19-29 °C), $\Delta T_{0.1-1.1}$ (<3 °C), and ΔT_{pr} (<10 °C), as well as their PDs (≤10%, ≤5%, and ≤5%, respectively). Figure **19** presents the hourly

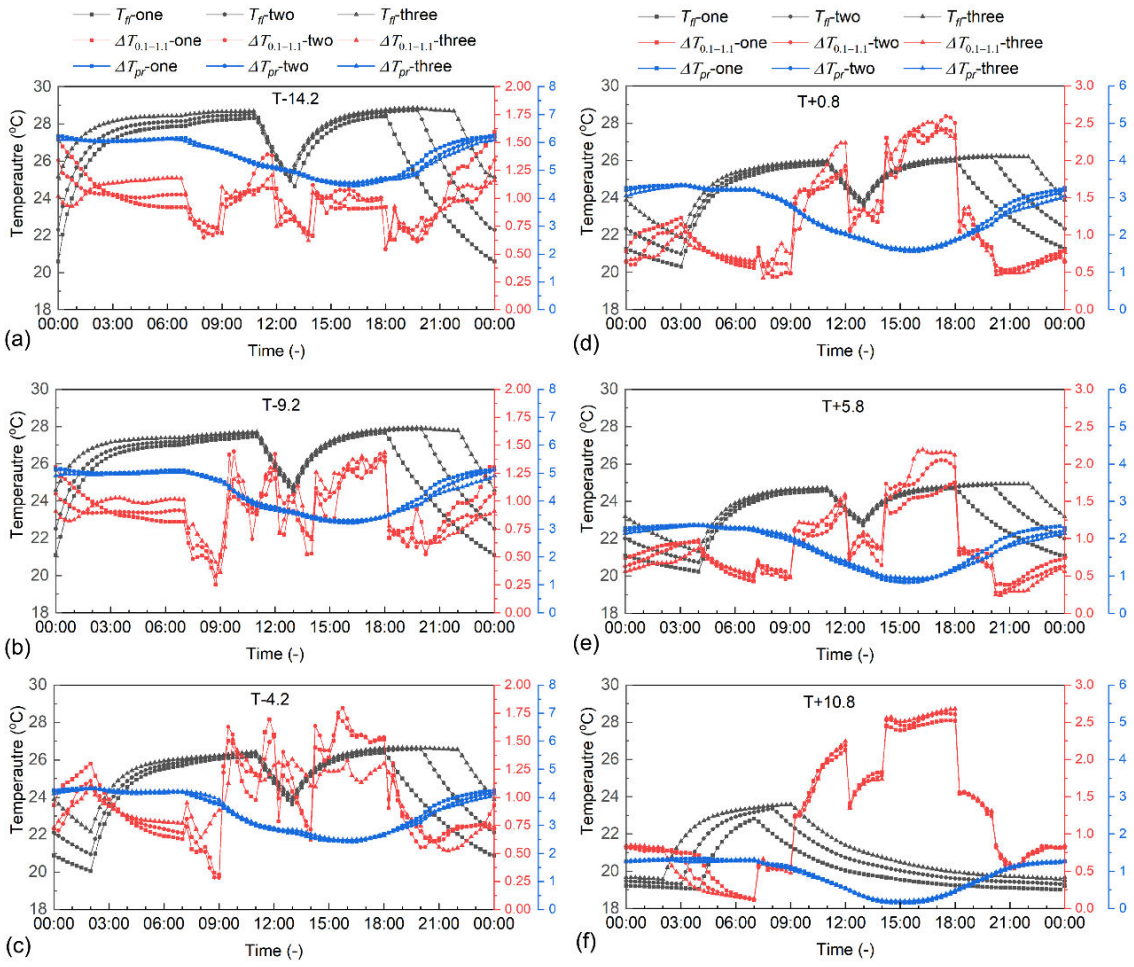

Figure 19: Hourly variations of T_{fl}, $\Delta T_{0.1-1.1}$, and ΔT_{pr} under six different control strategies: (a) $T_{min,out1}$ = -14.2 °C; (b) $T_{min,out2}$ = -9.2 °C; (c) $T_{min,out3}$ = -4.2 °C; (d) $T_{min,out4}$ = 0.8 °C; (e) $T_{min,out5}$ = 5.8 °C; (f) $T_{min,out6}$ = 10.8 °C.

variations of T_{fl}, $\Delta T_{0.1-1.1}$, and ΔT_{pr} under different control strategies. The value of T_{fl} in all cases was maintained in the range of 20 °C to 28 °C, except for the cases of $T_{min,out}$ = -14.2 °C and $T_{min,out}$ = 10.8 °C, which had the maximum floor temperatures up to about 29.1 °C and the minimum floor temperatures down to about 18.9 °C. It was also found that, due to the intermittent starting and stopping of the water supply, the profiles of the floor temperature are characterized by a gradually increasing variation before working hours and a decreasing trend after working hours, as well as a sudden change presenting as a V-shape at noon. Moreover, they apparently exhibit significant differences under different water supply schedules; the shorter the daily period of the water supply, the lower the floor surface temperature.

For $\Delta T_{0.1-1.1}$, only the cases when $T_{min,out}$ was equal to 0.8 °C, 5.8 °C, and 10.8°C presented slightly higher values ranging from 2.2 °C to 2.6 °C. The difference is mainly linked to the lower air supply temperature during the working period, which was originally designed to reduce the pre-heating period and energy consumption. Although the variations were found to decrease or increase remarkably, while those of $\Delta T_{0.1-1.1}$ remained in the scope of the thermal comfort criteria, the overall performance was acceptable.

Regarding ΔT_{pr}, fewer discrepancies were observed among all three cases under the same value of $T_{min,out}$. Moreover, the maximum ΔT_{pr} of about 6.5 °C occurred in the case of $T_{min,out}$ = -14.2 °C, which is within the standard required scope. Therefore, the effect of ΔT_{pr} on thermal comfort is acceptable.

Figure **20** presents the box plots for the PDs due to T_{fl}, $\Delta T_{0.1-1.1}$, and ΔT_{pr} under different control strategies. Because the same scales of PD were identified for $\Delta T_{0.1-1.1}$ and ΔT_{pr}, as shown on the right Y-axis, a remarkable difference was that a negligible effect of $PD_{\Delta Tpr}$ was obtained as compared with $PD_{\Delta T0.1-1.1}$. However, $PD_{\Delta T0.1-1.1}$ also remained within a relatively

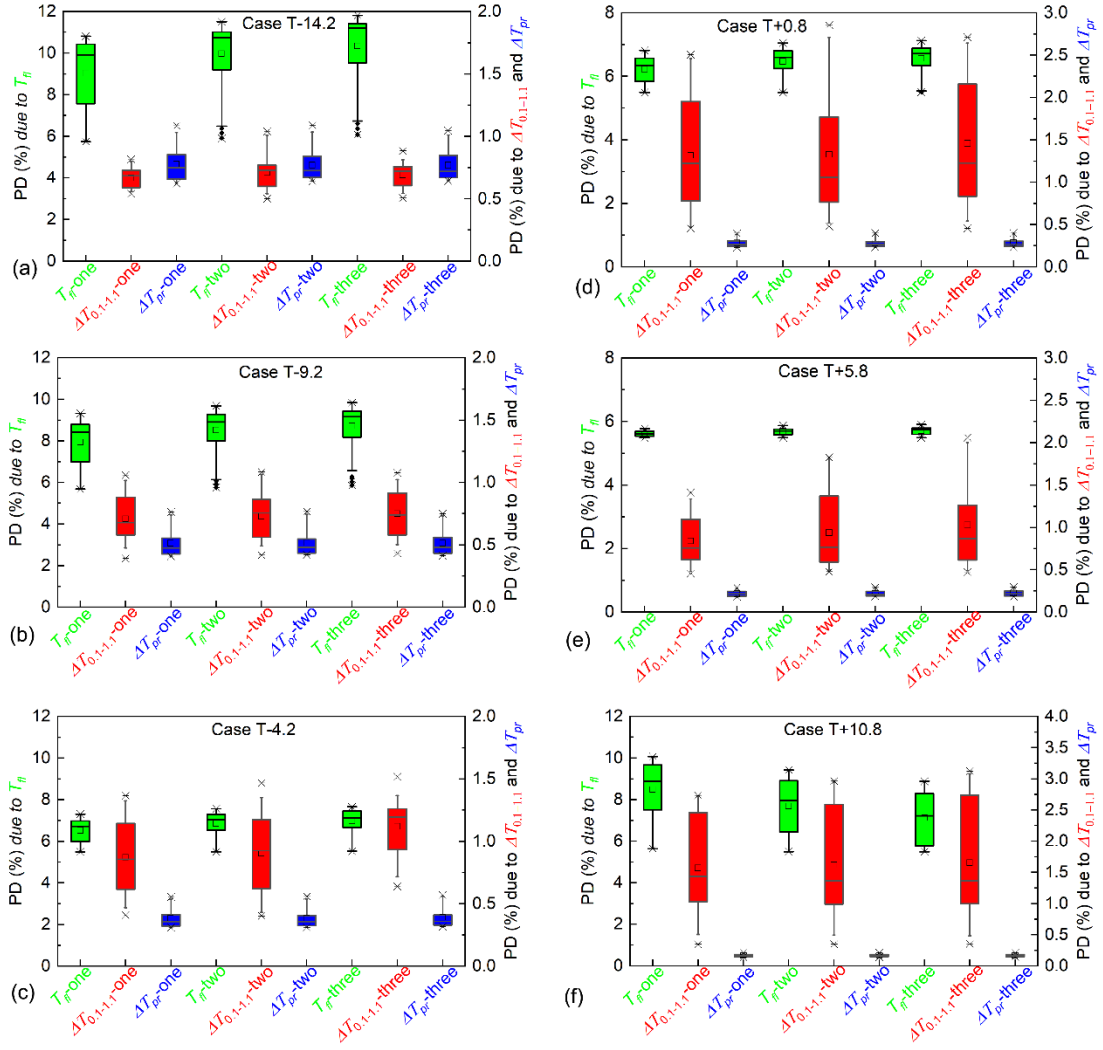

Figure 20: Box plots for PD due to T_{fl}, $\Delta T_{0.1-1.1}$, and ΔT_{pr} under different control strategies: (a) $T_{min,out1}$ = -14.2 °C; (b) $T_{min,out2}$ = -9.2 °C; (c) $T_{min,out3}$ = -4.2 °C; (d) $T_{min,out4}$ = 0.8 °C; (e) $T_{min,out5}$ = 5.8 °C; (f) $T_{min,out6}$ = 10.8 °C.

small range with a maximum value of 3.2% for the case of $T_{min,out}$ = 10.8 °C.

According to the figure, PD_{Tfl} may play a significant role in determining the control strategies. A trade-off between the PD and operative temperature must be selected, especially for the case of $T_{min,out}$ = -14.2 °C, as the other cases displayed acceptable performance. While the aforementioned case in which the water supply was shut off after 20:00 and was turned on again at 00:00 ensured a better temperature at 07:00, a higher PD was observed, as shown in Figure (**20a**). This is due to the higher floor temperature during the period 14:00-18:00, as the assumption of a sufficient indoor heat gain contributed to this performance.

Based on the control trade-off identified thus far, the optimized schedules yielding the acceptable thermal comfort performance in the intermittent operating mode of a floor heating system were ultimately defined, as reported in Table **9**. The results demonstrate the feasibility of using $T_{min,out}$ and T_{ave} as control indices in six different outdoor climatic conditions. A negative

Table 9: Optimal Floor-Heating Schedules for Designed $T_{min,out}$.

$T_{min,out}$ (°C)	Heating Schedule	T_{ave} (°C)
≤-15	All day on	35.0
-14.2	0:00-11:00, 13:00-20:00	34.7
-9.2	0:00-11:00, 13:00-18:00	33.1
-4.2	02:00-11:00, 13:00-20:00	31.4
0.8	03:00-11:00, 13:00-18:00	29.7
5.8	04:00-11:00, 13:00-18:00	28.1
10.8	02:00-09:00	26.4
>15	All day off	-

linear correlation between T_{ave} and $T_{min,out}$ was proven after taking into account the heating schedules. The shutting off of the water supply for 2 hours at noon and at least 4 hours during the nighttime was ultimately selected to maintain an acceptable indoor thermal environment and effectively reduce the energy consumption.

3.4. The Effect of Solar Radiation on the Indoor Thermal Environment

To indicate the effect of solar radiation, $T_{sol\text{-}air}$ was employed to consider the effect of the heat gained by exterior surfaces. Figure **21** depicts the hourly variation of $T_{sol\text{-}air}$ for the roof, walls, and windows under two different direct solar radiation conditions, and remarkable differences were observed. Maximum temperatures of 8.6 °C and 2.1°C for the wall surfaces were achieved due to the effects of solar radiation of 736 W/m^2 and 446 W/m^2, respectively, in contrast to the maximum temperature of -6.5 °C achieved without the effect of solar radiation.

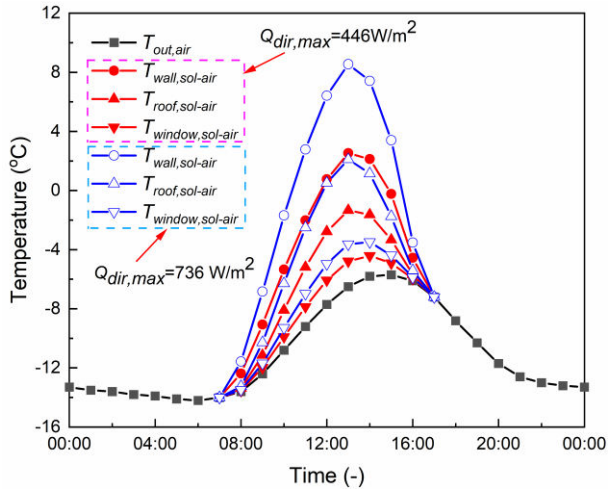

Figure 21: Hourly variation of $T_{sol\text{-}air}$ for the roof, walls, and windows under different effects of maximum Q_{dir}.

According to Table **7**, three cases with different direct solar radiation values and heating schedules within the range of -15 °C < $T_{min,out}$ ≤ -10 °C are proposed. Note that the air supply and infiltration boundary conditions are same as the previous simulation cases that neglected the effect of solar radiation. Figure **22** presents the temperature variations of the interior surfaces, including the windows, ceiling, and walls. A noticeable discrepancy was observed between the temperatures of the surfaces of the walls, ceiling, and windows due to the different effects of solar radiation. Under the effect of the thermal inertia of the building envelope, the wall and ceiling had relatively longer thermal storage and release processes and maintained stable changes, whereas that of the window surface varied slightly only during the daytime, especially during the period of the occurrence of solar radiation.

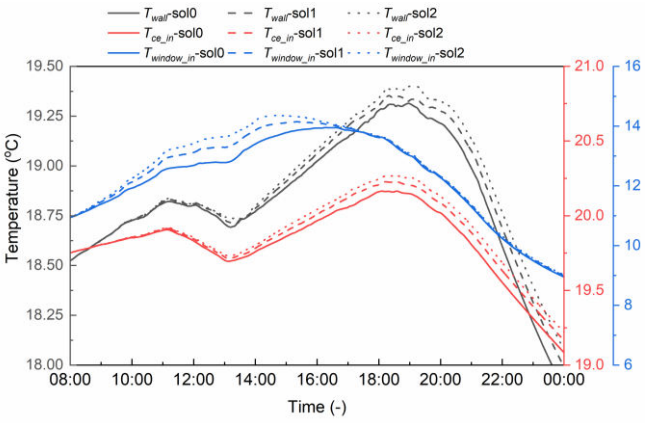

Figure 22: Hourly temperature variations of interior surfaces including the windows, ceiling, and walls affected by solar radiation.

The maximum temperature differences for the wall, ceiling, and windows between Case sol1 and Case sol0 were 0.11 °C, 0.08 °C, and 0.53 °C, respectively, whereas the differences between Case sol1 and Case sol0 were 0.20 °C, 0.14 °C, and 0.87 °C, respectively; moreover, the maximum temperature differences occurred at 00:00, 00:00, and 13:12, respectively. It must be noted that the temperature differences were minimal due to the better insulation levels of the wall and ceiling structures.

To comprehensively compare the differences of the indoor thermal parameters, the temperatures of the interior surfaces, the operative temperature, and the air temperature at the height of 1.1 m during the working period are summarized in Table **10**. Unremarkable differences were found, excluding those for the internal window surface. The differences of $T_{1.1}$ and T_{op} over time remained stable; therefore, a negligible thermal comfort difference can be concluded while only considering the heat transfer function as affected by solar radiation. In other words, in future studies, the

Table 10: Maximum Temperature Differences (°C) between Cases with and without the Solar Radiation Effect During the Working Period (07:00-20:00)

Case	T_{ce}	T_w	T_{window}	T_{fl}	$T_{1.1}$	T_{op}
$\Delta T_{sol1\text{-}sol0}$	0.07	0.09	0.52	0.03	0.07	0.09
$\Delta T_{sol2\text{-}sol0}$	0.12	0.14	0.87	0.07	0.11	0.13

effect of solar radiation from the incident sunlight transmitted from windows on the floor surface must be taken into account under the condition of a better insulation level of the building envelope.

4. DISCUSSION

Overall, this study provided control strategies for a radiant floor heating system based on minimum outdoor air temperature to maintain an acceptable indoor thermal comfort environment. Due to the requirement of an accurate setup of complicated outdoor/indoor climatic conditions for the numerical method, some specifically-designed assumptions were defined. For example, the hourly-varying outdoor air temperature was selected based on data on typical winter weather used in the EnergyPlus simulation program. The maximum daily temperature difference of about 8.5 ^{o}C was predefined and smaller temperature differences, e.g., within 2~4 ^{o}C, were not accounted for.

Moreover, the indoor heat gains, including the occupants, the equipment load, and the lighting gains, were assumed to be uniformly distributed with a volumetric heat generation varying with a step change over time. In realistic conditions, continuous changes may achieve a relatively accurate performance. Although the heat gains of the exterior surfaces of the building envelope were considered, the heat gains on the floor surface from the incident sunlight transmitted from windows should be taken into account [29, 80]. This is the drawback of this study and may require a complicated process due to the unstable locations affected by sunlight in the transient simulation.

Also, the present numerical simulation only considered the weekday operating schedules of floor-heating; however, the control strategies for weekend schedules may require additional serious considerations, because the outdoor/indoor climatic conditions, as well as their load schedules, significantly affect the indoor thermal environment. Finally, as a CFD study, the boundary conditions were assumed to be in a stable mode or limited to a small number of cases, e.g., the inlet ventilation cases, in addition to the previously mentioned disadvantages. Under realistic conditions, a variable air volume system may be used for most occasions. However, these are all attributed to the predefined process of CFD, instead of the interactive process in a transient simulation; therefore, in future studies, data communication must be introduced for model predictive controls.

5. CONCLUSION

A 2D numerical study was conducted to evaluate the thermal comfort performance in a radiant floor heating system combined with a displacement ventilation system while taking into account the intermittent operating strategies on weekdays. The varying outdoor air temperature and indoor heat gains, as well as infiltration ventilation during the unoccupied period, were designed and set up in CFD simulation cases. The operative temperature, vertical air temperature, floor temperature, and radiant asymmetry, as well as the corresponding percentages dissatisfied, were used as the evaluation criteria of thermal comfort. The results demonstrate the feasibility of using $T_{min,out}$ and T_{ave} as control indices under six different outdoor climatic conditions ($T_{min,out}$ = -14.2 ^{o}C, -9.2 ^{o}C, 4.2 ^{o}C, 0.8 ^{o}C, 5.8 ^{o}C, and 10.8 ^{o}C, respectively). A control strategy with the alteration of T_{ave} is ultimately obtained according to the varying value of $T_{min,out}$ in the range of -15 ^{o}C < $T_{min,out}$ ≤ 15 ^{o}C, which featured a negative linear correlation between the previously mentioned parameters.

Results show that for the case with a minimum outdoor air temperature of -14.2 ^{o}C, the earlier shut-off of the water supply (e.g., 18:00) cannot contribute to maintaining a comfortable environment at 7:00. To eliminate the effect of the indoor heat gain, a water supply shut-off after 20:00 and the pump starting to recirculate water in the concrete slab at 00:00 are encouraged in the case of an insufficient indoor heat gain during the next daytime. A trade-off between the percentages dissatisfied and the operative temperature is finally identified. The shut-off of the water supply for 2 hours at noon and at least 4 hours during the nighttime were also discerned to maintain an acceptable indoor thermal environment and effectively reduce energy consumption. Ultimately, although the heat gains of the exterior surfaces of the building envelope due to the effects of different solar radiation are considered, the maximum temperature differences for the wall, ceiling, and windows are not too large with about 0.20 ^{o}C, 0.14 ^{o}C, and 0.87 ^{o}C and occur at 00:00, 00:00, and 13:12, respectively, revealing the better insulation levels of the wall and ceiling structures. Further studies should take into account the heat gains of the floor surface from the incident sunlight transmitted from windows.

CONFLICTS OF INTEREST

The authors declare no potential conflicts of interest with respect to the research, authorship, and/or publication of this article.

ACKNOWLEDGEMENTS

This work was supported by the Support Plan for Outstanding Youth Innovation Team in Shandong Province (2019KJG005), National Natural Science Foundation of Shandong Province (ZR2020ME211), and and National Natural Science Foundation of China (51608310).

HIGHLIGHTS

A transient two-dimensional CFD model of a radiant floor heating system with a ventilation system is constructed.

Transient indoor thermal comfort conditions under different control strategies are numerically evaluated.

The intermittent controls based on the minimum outdoor air temperature and the average water supply and return temperature are proposed.

NOMENCLATURE

h_{ceil} = convective heat transfer coefficients for the ceiling (W/m^2·K)

h_{ext} = external surface convective heat transfer coefficient (W/m^2·K)

h_{int} = internal surface convective heat transfer coefficient (W/m^2·K)

h_{surf} = convective heat transfer coefficient of the interior/exterior surface (W/m^2·K)

h_{water} = convective heat transfer coefficient of the inner surface of the pipe (W/m^2·K)

k_{cover} = thermal conductivity of the cover layer

q_{source} = volumetric heat generation rate (W/m^2)

Q_{dir} = direct solar radiation (W/m^2)

$Q_{dir,max}$ = maximum direct solar radiation (W/m^2)

u_{in} = inlet air supply velocity (m/s)

T_{ave} = average water supply and return temperature (^{o}C)

T_{fl} = floor surface temperature (^{o}C)

T_{free} = free-stream temperature of surrounding fluid (^{o}C)

T_{in} = inlet air temperature (^{o}C)

$T_{min,out}$ = minimum outdoor air temperature (^{o}C)

T_{mrt} = mean radiant temperature (^{o}C)

T_{op} = operative temperature (^{o}C),

T_{out} = outdoor air temperature (^{o}C)

$T_{sol-air}$ = sol-air temperature (^{o}C)

T_{surf} = temperature of interior/exterior surfaces (^{o}C)

REFERENCES

[1] T. Alves, L. Machado, R.G. de Souza, P. de Wilde, A methodology for estimating office building energy use baselines by means of land use legislation and reference buildings, Energy Build. 143 (2017) 100-113. https://doi.org/10.1016/j.enbuild.2017.03.017

[2] J. Liu, M. Heidarinejad, S. Gracik, D. Jareemit, J. Srebric, The impact of surface convective heat transfer coefficients on the simulated building energy consumption and surface temperatures The 13th International Conference on Indoor Air Quality and Climate, Hong Kong, 2014.

[3] M. Economidou, V. Todeschi, P. Bertoldi, D. D'Agostino, P. Zangheri, L. Castellazzi, Review of 50 years of EU energy efficiency policies for buildings, Energy Build. 225 (2020) 110322. https://doi.org/10.1016/j.enbuild.2020.110322

[4] J. Srebric, M. Heidarinejad, J. Liu, Building neighborhood emerging properties and their impacts on multi-scale modeling of building energy and airflows, Build. Environ. 91 (2015) 246-262. https://doi.org/10.1016/j.buildenv.2015.02.031

[5] A.R. Amaral, E. Rodrigues, A. Rodrigues Gaspar, Á. Gomes, Review on performance aspects of nearly zero-energy districts, Sust. Cities Soc. 43 (2018) 406-420. https://doi.org/10.1016/j.scs.2018.08.039

[6] L. Pérez-Lombard, J. Ortiz, C. Pout, A review on buildings energy consumption information, Energy Build. 40(3) (2008) 394-398. https://doi.org/10.1016/j.enbuild.2007.03.007

[7] K.-N. Rhee, K.W. Kim, A 50 year review of basic and applied research in radiant heating and cooling systems for the built environment, Build. Environ. 91 (2015) 166-190. https://doi.org/10.1016/j.buildenv.2015.03.040

[8] C. Zhang, M. Pomianowski, P.K. Heiselberg, T. Yu, A review of integrated radiant heating/cooling with ventilation systems-Thermal comfort and indoor air quality, Energy Build. 223 (2020) 110094. https://doi.org/10.1016/j.enbuild.2020.110094

[9] P. Mustakallio, Z. Bolashikov, L. Rezgals, A. Lipczynska, A. Melikov, R. Kosonen, Thermal environment in a simulated double office room with convective and radiant cooling systems, Build. Environ. 123 (2017) 88-100. https://doi.org/10.1016/j.buildenv.2017.06.029

[10] P. Mustakallio, Z. Bolashikov, K. Kostov, A. Melikov, R. Kosonen, Thermal environment in simulated offices with convective and radiant cooling systems under cooling (summer) mode of operation, Build. Environ. 100 (2016) 82-91. https://doi.org/10.1016/j.buildenv.2016.02.001

[11] M.A. Hassan, O. Abdelaziz, Best practices and recent advances in hydronic radiant cooling systems - Part II: Simulation, control, and integration, Energy Build. 224 (2020) 110263. https://doi.org/10.1016/j.enbuild.2020.110263

[12] M. Schmelas, T. Feldmann, E. Bollin, Savings through the use of adaptive predictive control of thermo-active building systems (TABS): A case study, Appl. Energy 199 (2017) 294-309. https://doi.org/10.1016/j.apenergy.2017.05.032

[13] J. Romaní, A. de Gracia, L.F. Cabeza, Simulation and control of thermally activated building systems (TABS), Energy Build. 127 (2016) 22-42. https://doi.org/10.1016/j.enbuild.2016.05.057

[14] S.-B. Leigh, C. MacCluer, Comparative study of proportional flux-modulation and various types of temperature-modulation approaches for radiant floor-heating system control, ASHRAE Transactions 100(1) (1994) 1040-1053.

[15] L. Zhang, X. Huang, L. Liang, J. Liu, Experimental study on heating characteristics and control strategies of ground source heat pump and radiant floor heating system in an office building, Procedia Engineering 205 (2017) 4060-4066. https://doi.org/10.1016/j.proeng.2017.09.890

[16] H. Tang, P. Raftery, X. Liu, S. Schiavon, J. Woolley, F.S. Bauman, Performance analysis of pulsed flow control method for radiant slab system, Build. Environ. 127 (2018) 107-119. https://doi.org/10.1016/j.buildenv.2017.11.004

[17] L. Zhang, H. Li, J. Liu, M.K. Kim, L. Zhang, Simulation and control of radiant floor cooling systems: intermittent operation and weather-forecast-based predictive controls, IOP Conference Series: Materials Science and Engineering 609 (2019) 062006. https://doi.org/10.1088/1757-899X/609/6/062006

[18] S.H. Cho, M. Zaheer-uddin, Predictive control of intermittently operated radiant floor heating systems, Energy Conv. Manag. 44(8) (2003) 1333-1342. https://doi.org/10.1016/S0196-8904(02)00116-4

[19] G. Yeom, D.E. Jung, S.L. Do, Improving a Heating Supply Water Temperature Control for Radiant Floor Heating Systems in Korean High-Rise Residential Buildings, Sustainability 11(14) (2019) 3926. https://doi.org/10.3390/su11143926

[20] M.-S. Shin, K.-N. Rhee, G.-J. Jung, Optimal heating start and stop control based on the inferred occupancy schedule in a household with radiant floor heating system, Energy Build. 209 (2020) 109737. https://doi.org/10.1016/j.enbuild.2019.109737

[21] M. Gwerder, J. Tödtli, B. Lehmann, V. Dorer, W. Güntensperger, F. Renggli, Control of thermally activated building systems (TABS) in intermittent operation with pulse width modulation, Appl. Energy 86(9) (2009) 1606-1616. https://doi.org/10.1016/j.apenergy.2009.01.008

[22] J.-Y. Lee, M.-S. Yeo, K.-W. Kim, Predictive Control of the Radiant Floor Heating System in Apartment Buildings, Journal of Asian Architecture and Building Engineering 1(1) (2002) 105-112. https://doi.org/10.3130/jaabe.1.105

[23] W. Jin, J. Ma, L. Jia, Z. Wang, Dynamic variation of surface temperatures on the radiant ceiling cooling panel based on the different supply water temperature adjustments, Sust. Cities Soc. 52 (2020) 101805. https://doi.org/10.1016/j.scs.2019.101805

[24] F. Causone, F. Baldin, B.W. Olesen, S.P. Corgnati, Floor heating and cooling combined with displacement ventilation: Possibilities and limitations, Energy Build. 42(12) (2010) 2338-2352. https://doi.org/10.1016/j.enbuild.2010.08.001

[25] Z. Zhai, Application of Computational Fluid Dynamics in Building Design: Aspects and Trends, Indoor Built Environ. 15(4) (2006) 305-313. https://doi.org/10.1177/1420326X06067336

[26] K. Zhao, X.-H. Liu, Y. Jiang, Application of radiant floor cooling in large space buildings - A review, Renew. Sust. Energ. Rev. 55 (2016) 1083-1096. https://doi.org/10.1016/j.rser.2015.11.028

[27] Y. Zhu, M. Luo, Q. Ouyang, L. Huang, B. Cao, Dynamic characteristics and comfort assessment of airflows in indoor environments: A review, Build. Environ. 91 (2015) 5-14. https://doi.org/10.1016/j.buildenv.2015.03.032

[28] J. Liu, S. Zhu, M.K. Kim, J. Srebric, A Review of CFD Analysis Methods for Personalized Ventilation (PV) in Indoor Built Environments, Sustainability 11(15) (2019) 4166. https://doi.org/10.3390/su11154166

[29] Q. Dong, S. Li, C. Han, Numerical and experimental study of the effect of solar radiation on thermal comfort in a radiant heating system, J. Build. Eng. 32 (2020) 101497. https://doi.org/10.1016/j.jobe.2020.101497

[30] R. Gao, A. Li, O. Zhang, H. Zhang, Comparison of indoor air temperatures of different under-floor heating pipe layouts, Energy Conv. Manag. 52(2) (2011) 1295-1304. https://doi.org/10.1016/j.enconman.2010.09.027

[31] X. Zheng, Y. Han, H. Zhang, W. Zheng, D. Kong, Numerical study on impact of non-heating surface temperature on the heat output of radiant floor heating system, Energy Build. 155 (2017) 198-206. https://doi.org/10.1016/j.enbuild.2017.09.022

[32] J. Romaní, L.F. Cabeza, A. de Gracia, Development and experimental validation of a transient 2D numeric model for radiant walls, Renew. Energy 115 (2018) 859-870. https://doi.org/10.1016/j.renene.2017.08.019

[33] M. Tye-Gingras, L. Gosselin, Comfort and energy consumption of hydronic heating radiant ceilings and walls based on CFD analysis, Build. Environ. 54 (2012) 1-13. https://doi.org/10.1016/j.buildenv.2012.01.019

[34] H. Karabay, M. Arıcı, M. Sandık, A numerical investigation of fluid flow and heat transfer inside a room for floor heating and wall heating systems, Energy Build. 67 (2013) 471-478. https://doi.org/10.1016/j.enbuild.2013.08.037

[35] L. Zhang, J. Liu, M. Heidarinejad, M.K. Kim, J. Srebric, A Two-Dimensional Numerical Analysis for Thermal Performance of an Intermittently Operated Radiant Floor Heating System in a Transient External Climatic Condition, Heat Transf. Eng. 41(9-10) (2020) 825-839. https://doi.org/10.1080/01457632.2019.1576422

[36] EN ISO 7730, Ergonomics of the thermal environment - analytical determination and interpretation of thermal comfort using calculation of the PMV and PPD indices and local thermal comfort criteria, in: I.S. Organisation (Ed.) Geneva, Switzerland, 2005.

[37] J. Liu, J. Ren, L. Zhang, X. Xie, M.K. Kim, L. Zhang, Optimization of Control Strategies for the Radiant Floor Cooling System Combined with Displacement Ventilation: A Case Study of an Office Building in Jinan, China, Int. J. Archit. Eng. Technol. 6 (2019) 33-48. https://doi.org/10.15377/2409-9821.2019.06.5

[38] MHURD, Design standard for energy efficiency of public buildings (GB50189-2015), Ministry of Housing and Urban Rural Development of the People's Republic of China, Beijing, China, 2015.

[39] ANSYS Inc, ANSYS FLUENT Theory Guide, Release 16.1, Canonsburg, USA, 2014.

[40] F.R. Menter, Two-equation eddy-viscosity turbulence models for engineering applications, AIAA Journal 32(8) (1994) 1598-1605. https://doi.org/10.2514/3.12149

[41] B.E. Yuce, E. Pulat, Forced, natural and mixed convection benchmark studies for indoor thermal environments, International Communications in Heat and Mass Transfer 92 (2018) 1-14. https://doi.org/10.1016/j.icheatmasstransfer.2018.02.003

[42] J. Liu, D.A. Dalgo, S. Zhu, H. Li, L. Zhang, J. Srebric, Performance analysis of a ductless personalized ventilation combined with radiant floor cooling system and displacement ventilation, Build. Simul. 12(5) (2019) 905-919. https://doi.org/10.1007/s12273-019-0521-9

[43] H. Li, C. Xi, X. Kong, Z. Lin, L. Wang, A comparative experimental investigation on radiant floor heating system and stratum ventilation, Sust. Cities Soc. 52 (2020) 101823. https://doi.org/10.1016/j.scs.2019.101823

[44] B. Yang, A.K. Melikov, A. Kabanshi, C. Zhang, F.S. Bauman, G. Cao, H. Awbi, H. Wigö, J. Niu, K.W.D. Cheong, K.W. Tham, M. Sandberg, P.V. Nielsen, R. Kosonen, R. Yao, S. Kato, S.C. Sekhar, S. Schiavon, T. Karimipanah, X. Li, Z. Lin, A review of advanced air distribution methods - theory, practice, limitations and solutions, Energy Build. 202 (2019) 109359. https://doi.org/10.1016/j.enbuild.2019.109359

[45] J. Liu, Z. Li, M.K. Kim, S. Zhu, L. Zhang, J. Srebric, A comparison of the thermal comfort performances of a radiation floor cooling system when combined with a range of ventilation systems, Indoor Built Environ. 29(4) (2020) 527-542. https://doi.org/10.1177/1420326X19869412

[46] EN 15251, Indoor Environmental Input Parameters for Design and Assessment of Energy Performance of Buildings Addressing Indoor Air Quality, Thermal Environment, Lighting and Acoustics, in: E.C.f. Standardization (Ed.) Brussels, 2007.

[47] M. Krajčík, R. Tomasi, A. Simone, B.W. Olesen, Experimental udy including subjective evaluations of mixing and displacement ventilation combined with radiant floor heating/cooling system, HVAC&R RES. 19(8) (2013) 1063-1072. https://doi.org/10.1080/10789669.2013.806173

[48] R.A. Grot, A.K. Persily, Measured Air Infiltration and Ventilation Rates in Eight Large Office Buildings, in: H.R. Trechsel, P.L. Lagus (Eds.), ASTM International, West Conshohocken, PA, 1986, pp. 151-183. https://doi.org/10.1520/STP19647S

[49] Korolija, L. Marjanovic-Halburd, Y. Zhang, V.I. Hanby, UK office buildings archetypal model as methodological approach in development of regression models for predicting building energy consumption from heating and cooling demands, Energy Build. 60 (2013) 152-162. https://doi.org/10.1016/j.enbuild.2012.12.032

[50] D. VanBronkhorst, A. Persily, S. Emmerich, Energy impacts of air leakage in US office buildings, DOCUMENT-AIR INFILTRATION CENTRE AIC PROC, OSCAR FABER PLC, 1995, pp. 379-379.

[51] L.C. Ng, A. Musser, A.K. Persily, S.J. Emmerich, Multizone airflow models for calculating infiltration rates in commercial reference buildings, Energy Build. 58 (2013) 11-18. https://doi.org/10.1016/j.enbuild.2012.11.035

[52] W. Liu, X. Zhao, Q. Chen, A novel method for measuring air infiltration rate in buildings, Energy Build. 168 (2018) 309-318. https://doi.org/10.1016/j.enbuild.2018.03.035

[53] K. Ito, K. Inthavong, T. Kurabuchi, T. Ueda, T. Endo, T. Omori, H. Ono, S. Kato, K. Sakai, Y. Suwa, CFD benchmark tests for indoor environmental problems: Part 1 isothermal/non-isothermal flow in 2D and 3D room model, Int. J. Archit. Eng. Technol. 2(1) (2015) 1-22. https://doi.org/10.15377/2409-9821.2015.02.01.1

[54] K. Ito, K. Inthavong, T. Kurabuchi, T. Ueda, T. Endo, T. Omori, H. Ono, S. Kato, K. Sakai, Y. Suwa, CFD benchmark tests for indoor environmental problems: Part 2 cross-ventilation airflows and floor heating systems, Int. J. Archit. Eng. Technol. 2(1) (2015) 23-49. https://doi.org/10.15377/2409-9821.2015.02.01.2

[55] K. Ito, K. Inthavong, T. Kurabuchi, T. Ueda, T. Endo, T. Omori, H. Ono, S. Kato, K. Sakai, Y. Suwa, CFD benchmark tests for indoor environmental problems: Part 3 numerical thermal manikins, Int. J. Archit. Eng. Technol. 2(1) (2015) 50-75. https://doi.org/10.15377/2409-9821.2015.02.01.3

[56] K. Ito, K. Inthavong, T. Kurabuchi, T. Ueda, T. Endo, T. Omori, H. Ono, S. Kato, K. Sakai, Y. Suwa, CFD benchmark tests for indoor environmental problems: Part 4 air-conditioning airflows, residential kitchen airflows and fire-induced flow, Int. J. Archit. Eng. Technol. 2(1) (2015) 76-102. https://doi.org/10.15377/2409-9821.2015.02.01.4

[57] P.V. Nielsen, Fifty years of CFD for room air distribution, Build. Environ. 91 (2015) 78-90. https://doi.org/10.1016/j.buildenv.2015.02.035

[58] P.V. Nielsen, F. Allard, H.B. Awbi, L. Davidson, A. Schälin, Computational Fluid Dynamics in Ventilation Design REHVA Guidebook No 10, Taylor & Francis, 2007. https://doi.org/10.1080/14733315.2007.11683784

[59] S. Gilani, H. Montazeri, B. Blocken, CFD simulation of stratified indoor environment in displacement ventilation: Validation and sensitivity analysis, Build. Environ. 95 (2016) 299-313. https://doi.org/10.1016/j.buildenv.2015.09.010

[60] X. Wu, J. Zhao, B.W. Olesen, L. Fang, F. Wang, A new simplified model to calculate surface temperature and heat transfer of radiant floor heating and cooling systems, Energy Build. 105 (2015) 285-293. https://doi.org/10.1016/j.enbuild.2015.07.056

[61] X. Liu, T. Zhang, X. Zhou, H. Tang, Radiant cooling, China Architecture & Building Press, Beijing, China, 2019.

[62] MHURD, Technical Specification for Radiant Heating and Cooling (JGJ142-2012), Ministry of Housing and Urban Rural Development of the People's Republic of China, Beijing, China, 2012.

[63] J. Liu, X. Xie, F. Qin, S. Song, D. Lv, A case study of ground source direct cooling system integrated with water storage tank system, Build. Simul. 9(6) (2016) 659-668. https://doi.org/10.1007/s12273-016-0297-0

[64] BEERC, 2014 Annual Report on China Builidng Energy Efficiency. The Building Energy Efficiency Research Center of Tsinghua University, Beijing, China, 2014.

[65] J. Liu, M. Heidarinejad, S. Gracik, J. Srebric, The impact of exterior surface convective heat transfer coefficients on the building energy consumption in urban neighborhoods with different plan area densities, Energy Build. 86 (2015) 449-463. https://doi.org/10.1016/j.enbuild.2014.10.062

[66] G.N. Walton, Thermal Analysis Research Program Reference Manual (NBSSIR 83-2655), National Bureau of Standards, 1983. https://doi.org/10.6028/NBS.IR.83-2655

[67] P.V. Nielsen, S. Murakami, S. Kato, C. Topp, J.-H. Yang, Benchmark tests for a computer simulated person, Aalborg University, Indoor Environmental Engineering, (https://www.cfd-benchmarks.com/) (2003).

[68] Energyplus, EnergyPlus Engineering Reference, Ernest Orlando Lawrence Berkeley National Laboratory: Berkeley, CA, USA, 2017.

[69] J.-M. Choi, K.-N. Lee, S.-R. Ryu, Y.-Y. Kim, M.-S. Yeo, K.-W. Kim, A study on the required supply water temperature calculating method for the control of multizone radiant floor heating system, Korean Journal of Air-Conditioning and Refrigeration Engineering 19(1) (2007) 77-85.

[70] K. Zhao, X. Liu, J. Ge, Performance investigation of convective and radiant heat removal methods in large spaces, Energy Build. 208 (2020) 109650. https://doi.org/10.1016/j.enbuild.2019.109650

[71] H. Tang, T. Zhang, X. Liu, Y. Jiang, Novel method for the design of radiant floor cooling systems through homogenizing spatial solar radiation distribution, Sol. Energy 170 (2018) 885-895. https://doi.org/10.1016/j.solener.2018.06.039

[72] A.K. Athienitis, Y. Chen, The effect of solar radiation on dynamic thermal performance of floor heating systems, Sol. Energy 69(3) (2000) 229-237. https://doi.org/10.1016/S0038-092X(00)00052-9

[73] ASHRAE, ASHRAE Handbook-Fundamentals, American Society of Heating Airconditioning and Refrigeration Engineers, Atlanta, Atlanta, USA, 2005.

[74] P.O. Fanger, B.M. Ipsen, G. Langkilde, B.W. Olessen, N.K. Christensen, S. Tanabe, Comfort limits for asymmetric thermal radiation, Energy Build. 8(3) (1985) 225-236. https://doi.org/10.1016/0378-7788(85)90006-4

[75] B.W. Olesen, Radiant floor heating in theory and practice, Ashrae Journal 44(7) (2002) 19-26.

[76] F.R. d'Ambrosio Alfano, M. Dell'Isola, B.I. Palella, G. Riccio, A. Russi, On the measurement of the mean radiant temperature and its influence on the indoor thermal environment assessment, Build. Environ. 63 (2013) 79-88. https://doi.org/10.1016/j.buildenv.2013.01.026

[77] ASHRAE Standard 55, Thermal environmental Conditions for Human Occupancy, American Society of Heating, Refrigerating and Air-Conditioning Engineers, Atlanta, USA, 2004.

[78] D. Blay, Confined turbulent mixed convection in the presence of horizontal buoyant wall jet, HTD Vol.213, Fundamentals of Mixed Convection, ASME1992.

[79] J. Liu, L. Liang, W. Wang, F. Qin, L. Zhang, S. Song, Field study on the performance of intermittently operated radiant floor heating system in an office, CLIMA 2016 - proceedings of the 12th REHVA World Congress: volume 2. Aalborg: Aalborg University, Department of Civil Engineering, 2016.

[80] C. Beji, A. Merabtine, S. Mokraoui, A. Kheiri, J. Kauffmann, N. Bouaziz, Experimental study on the effects of direct sun radiation on the dynamic thermal behavior of a floor-heating system, Sol. Energy 204 (2020) 1-12. https://doi.org/10.1016/j.solener.2020.04.055

Received on 26-11-2020 Accepted on 25-12-2020 Published on 30-12-2020

DOI: https://doi.org/10.15377/2409-9821.2020.07.6